INTERNATIONAL JOURNAL FOR NUMERICAL METHODS IN ENGINEERING
Int. J. Numer. Meth. Engng 2013; **95**:121–144
Published online 3 June 2013 in Wiley Online Library (wileyonlinelibrary.com). DOI: 10.1002/nme.4499

A stable Galerkin reduced order model for coupled fluid–structure interaction problems

I. Kalashnikova[1,*,†], M. F. Barone[2] and M. R. Brake[3]

[1]*Numerical Analysis and Applications Department, Sandia National Laboratories, PO Box 5800, MS 1320, Albuquerque, NM 87185, USA*
[2]*Aerosciences Department, Sandia National Laboratories, PO Box 5800, MS 1124, Albuquerque, NM 87185, USA*
[3]*Component Science and Mechanics Department, Sandia National Laboratories, PO Box 5800, MS 1070, Albuquerque, NM 87185, USA*

SUMMARY

A stable reduced order model (ROM) of a linear fluid–structure interaction (FSI) problem involving linearized compressible inviscid flow over a flat linear von Kármán plate is developed. Separate stable ROMs for each of the fluid and the structure equations are derived. Both ROMs are built using the 'continuous' Galerkin projection approach, in which the continuous governing equations are projected onto the reduced basis modes in a continuous inner product. The mode shapes for the structure ROM are the eigenmodes of the governing (linear) plate equation. The fluid ROM basis is constructed via the proper orthogonal decomposition. For the linearized compressible Euler fluid equations, a symmetry transformation is required to obtain a stable formulation of the Galerkin projection step in the model reduction procedure. Stability of the Galerkin projection of the structure model in the standard L^2 inner product is shown. The fluid and structure ROMs are coupled through solid wall boundary conditions at the interface (plate) boundary. An *a priori* energy linear stability analysis of the coupled fluid/structure system is performed. It is shown that, under some physical assumptions about the flow field, the FSI ROM is linearly stable *a priori* if a stabilization term is added to the fluid pressure loading on the plate. The stability of the coupled ROM is studied in the context of a test problem of inviscid, supersonic flow past a thin, square, elastic rectangular panel that will undergo flutter once the non-dimensional pressure parameter exceeds a certain threshold. This *a posteriori* stability analysis reveals that the FSI ROM can be numerically stable even without the addition of the aforementioned stabilization term. Moreover, the ROM constructed for this problem properly predicts the maintenance of stability below the flutter boundary and gives a reasonable prediction for the instability growth rate above the flutter boundary. Copyright © 2013 John Wiley & Sons, Ltd.

Received 10 October 2012; Revised 1 March 2013; Accepted 13 March 2013

KEY WORDS: reduced order model (ROM); proper orthogonal decomposition (POD)/Galerkin projection; compressible Euler equations; von Kármán plate equation; linear numerical stability; flutter

1. INTRODUCTION

Despite the availability of an increasingly sophisticated collection of computational 'high-fidelity' finite element, finite volume, and finite difference codes for computing three-dimensional fluid flows, complex structural system dynamics, and the coupling of the two, these tools are in practice often too computationally expensive for use in a design or analysis setting. This situation has pushed researchers in mathematics and engineering applications to develop model reduction techniques. Reduced order models, or ROMs, are constructed from a high-fidelity simulation and retain the essential physics and dynamics of the high-fidelity model, but have a much lower computational cost

*Correspondence to: I. Kalashnikova, Numerical Analysis and Applications Department, Sandia National Laboratories, PO Box 5800, MS 1320, Albuquerque, NM 87185, USA.

†E-mail: ikalash@sandia.gov

and can thus be run in real or near real-time for use in applications that require on-the-spot decision-making, optimization, and/or control. Thus, ROMs can enable and enhance the understanding of fluid and structural systems at a relatively low computational cost.

In recent years, various approaches for building ROMs have been proposed. Many ROM techniques in fluid mechanics are derived from the proper orthogonal decomposition (POD)/ Galerkin projection approach [1–3]. Originally, this approach aimed to develop low-dimensional models containing only a few degrees of freedom (DoFs) to help enhance the understanding of the nonlinear dynamics of turbulent flows. Since then, other approaches to building fluid ROMs have been proposed, each with its own inherent strengths. Examples include the reduced basis method [4], balanced truncation [5,6], balanced POD [7,8], and goal-oriented ROMs [9]. Various techniques to reduce the number of DoFs of structural models have been proposed as well. One approach of model reduction methods for structures is to first develop a full finite element model, then use a component mode synthesis approach to significantly reduce the number of DoFs while incorporating the essential physics of the system, including nonlinearities [10–13]. Other methods include the use of a Galerkin approximation based on the results of a finite element analysis [14] and hierarchical finite element methods. In the latter approach, the order of the approximating polynomial is increased while the mesh size is held constant, which can allow for plate meshes with as little as one element [15, 16].

The use of ROMs in a predictive setting raises some fundamental questions regarding their numerical properties, namely their consistency, stability, and convergence. In the present work, attention is focused on the second of these properties, namely stability. It is well-known that the model reduction method known as balanced truncation [5, 6] has a rigorous stability guarantee. However, the computational cost of this method, which requires the computation and simultaneous diagonalization of infinite controllability and observability Gramians, makes balanced truncation computationally intractable for systems of very large dimensions. Less costly model reduction approaches such as the balanced POD method [7, 8], and the POD method [1–3] lack, in general, an *a priori* stability guarantee. That is, it is unknown *a priori* if a ROM constructed using these methods will preserve the stability properties of the high fidelity system from which the model was constructed. The stability of the reduced model is commonly evaluated *a posteriori*: the ROM is constructed, used to predict some dynamical behavior, and subsequently deemed a success if the solutions generated by the ROM are numerically stable and accurately reproduce the expected behavior. There is some risk inherent in this sort of analysis. A compressible fluid ROM might be stable for a given number of modes, but unstable for other choices of basis size, as shown in [9] for a POD model. If the underlying ROM possesses some numerical instability inconsistent with a physical instability exhibited by the system, for example, flutter in aeroelastic applications, it may predict the onset of the physical instability incorrectly. It would be desirable, therefore, to construct a ROM in a way that can ensure *a priori* that the discretization does not introduce any non-physical instabilities into the approximation.

The importance of obtaining a stable ROM has been recognized in recent years by a number of authors. The stability preserving model reduction approaches found in the literature fall into roughly two categories: approaches which derive (*a priori*) a stability-preserving model reduction framework that is specific to a particular equation set and approaches which stabilize an unstable ROM through a post-processing (*a posteriori*) stabilization step applied to an unstable algebraic ROM system. Both families of approaches have their inherent strengths and weaknesses. The former family of approaches typically requires access to the governing partial differential equations (PDEs) and can therefore be seen as intrusive (or embedded). However, these methods, by construction, ensure that the ROM respects the physics of the governing PDEs. In contrast, the latter family of approaches are less intrusive, as they are 'black box' in character, but may alter the physics inherent in the discretized equations, thereby affecting the accuracy of the ROM.

Examples of the former ROM stabilization approach include the work of Rowley *et al.* [17], Barone *et al.* [18, 19], and Serre *et al.* [20]. In [17], Rowley *et al.* show that Galerkin projection preserves the stability of an equilibrium point at the origin if an 'energy-based' inner product is employed. In [18, 19], Barone *et al.* demonstrate that a symmetry transformation leads to a stable formulation for a Galerkin ROM for the linearized, compressible Euler equations [18, 19], and

DOI: 10.1002/nme

nonlinear compressible Navier–Stokes equations [21] with solid wall and far-field boundary conditions. In [20], Serre *et al.* propose applying the stabilizing projection developed by Barone *et al.* in [18, 19] to a skew-symmetric system constructed by augmenting a given linear system with its adjoint system. This approach yields a ROM that is stable at finite time even if the energy of the physical model is growing. Examples of the latter ROM stabilization approach include the work of Amsallem *et al.* [22] and Bond *et al.* [23]. In [22], a method for stabilizing projection-based linear ROMs through the solution of a small-scale convex optimization problem is proposed. In [23], a set of linear constraints for the left-projection matrix, given the right-projection matrix, are derived to yield a projection framework that is guaranteed to generate a stable ROM. In both References [22] and [23], the authors choose to modify minimally the ROM, so that the physics are not drastically altered.

The present work addresses the numerical stability, in the spirit of the first family of ROM stabilization approaches described in the previous paragraph, of a linear coupled fluid–structure interaction (FSI) ROM involving compressible inviscid fluid flow over a structure. The fluid and structural ROMs are developed independently of each other, then combined into a single ROM using the appropriate boundary conditions. A survey of the literature reveals that the approach of performing the model reduction separately for the individual fluid and structural subsystems is common in the area of FSI [24–27]. This approach has several advantages: it keeps the number of parameters required in the ROM to a minimum (e.g., the fluid ROM need not depend on structural response parameters such as the dynamic pressure), and it allows one to take advantage of existing analysis capabilities in formulating the ROM (e.g., structural eigenmodes can be obtained for 'free', as they are routinely available in structural dynamics codes). Also common for FSI problems that arise in computational fluid dynamics (CFD) applications such as flutter analysis are ROMs based on the Arbitrary Lagrangian–Eulerian (ALE) [28] framework. In [25, 26], Lieu *et al.* demonstrate the potential of POD-based reduced order modeling for near real-time aeroelastic modeling of a complete F-16 fighter configuration in which the aeroelastic system is represented by a three-field ALE formulation. The ALE method is particularly well suited for problems with moving boundaries and large volume changes in the computational domain, but is beyond the scope of the present paper, which focuses on a linear fluid model with linearized boundary conditions.

The remainder of this paper is organized. The fluid ROM, constructed for the three-dimensional compressible Euler equations linearized about a steady base state using the POD/Galerkin projection approach [1–3], is described in Section 2. An energy stability analysis carried out for Galerkin methods applied to the linearized Euler equations [18, 19] reveals that the numerical stability of the ROM for these equations is intimately tied to the choice of inner product used to define the Galerkin projection. The result is the construction of an inner product for the fluid equations that guarantees certain *a priori* stability bounds satisfied by the ROM for *any* choice of basis using Galerkin projection. Section 3 details the ROM for the structure, a panel on an aircraft or some other moving body coupled to the adjacent supersonic compressible fluid flow; the displacement of which is described using linearized von Kármán plate theory. The out-of-plane displacement of the plate is expanded in a basis of eigensolutions to the governing linearized equation, and a Galerkin method is used to develop an equation of motion in terms of the modal coefficients. This coupling of the fluid and structure ROMs described previously through boundary condition terms is presented in Section 4. The coupling of the ROMs gives rise to a linear dynamical system, the numerical stability of which can be examined *a priori* and analytically using the energy method and the method of Lyapunov [29, 30]. The *a priori* stability analysis of the FSI ROM is facilitated by the fact that both the fluid and structure ROMs are constructed via the continuous projection approach as follows: the continuous PDEs, rather than a discretization of these equations, are projected onto the reduced modes. With this approach, the stability properties of the continuous PDEs carry over to the discrete Galerkin scheme. If an acoustically reflecting (or no-penetration) boundary condition is imposed on the fluid variables at the plate, numerical stability can be proven for the resulting coupled fluid/structure ROM system when a stabilization term is added to the pressure load applied on the plate and under certain physical assumptions. The performance of the proposed FSI ROM is evaluated numerically on a problem of inviscid, supersonic flow past a thin, square, elastic plate that undergoes flutter once the non-dimensional dynamic pressure parameter exceeds a

DOI: 10.1002/nme

certain threshold in Section 5. For this example, it is found that the ROM solution compares well with the theoretical result from quasi-steady aerodynamic theory ('piston theory' [24]), and remains stable below the flutter boundary. Conclusions are offered in Section 6.

2. FLUID REDUCED ORDER MODEL OF LINEARIZED COMPRESSIBLE FLOW

In the previous works [18,19], ROMs based on the POD/Galerkin projection method were developed as an alternative discretization of the linearized compressible Euler equations. The fluid ROM was built by first calculating a reduced basis using the POD of an ensemble of flow field realizations, and then taking the Galerkin projection of the governing (continuous) PDEs onto the basis of POD modes using an appropriate, carefully constructed inner product. To keep this article self-contained, the equations and model reduction approach for the fluid side of the FSI model are reviewed in this section.

2.1. Linearized Euler equations for compressible flow

Let

$$\mathbf{q}^{\mathrm{T}} \equiv \begin{pmatrix} u_1, & u_2, & u_3, & \zeta, & p \end{pmatrix} \in \mathbb{R}^5, \tag{1}$$

denote the vector of fluid state variables. Here, u_1, u_2, and u_3 are, respectively, the x_1, x_2, and x_3 components of the velocity vector $\mathbf{u}^{\mathrm{T}} \equiv \begin{pmatrix} u_1, & u_2, & u_3 \end{pmatrix}$, p is the fluid pressure, and $\zeta \equiv 1/\rho$ is the specific volume of the fluid (ρ denoting the fluid density).

The governing fluid equations are taken to be the compressible Euler equations, linearized about a steady base (or mean) state $\bar{\mathbf{q}}$. Splitting the state variable vector $\mathbf{q}$ into a steady mean plus a time-varying fluctuation ($\mathbf{q}(\mathbf{x},t) = \bar{\mathbf{q}}(\mathbf{x}) + \mathbf{q}'(\mathbf{x},t)$), this linearization results in a system of the form [31,32]

$$\frac{\partial \mathbf{q}'}{\partial t} + \underbrace{\mathbf{A}_i \frac{\partial \mathbf{q}'}{\partial x_i} + \mathbf{C}\mathbf{q}'}_{\equiv \mathscr{L}\mathbf{q}'} = \mathbf{0}, \tag{2}$$

where

$$\mathbf{A}_1 = \begin{pmatrix} \bar{u}_1 & 0 & 0 & 0 & \bar{\zeta} \\ 0 & \bar{u}_1 & 0 & 0 & 0 \\ 0 & 0 & \bar{u}_1 & 0 & 0 \\ -\bar{\zeta} & 0 & 0 & \bar{u}_1 & 0 \\ \gamma\bar{p} & 0 & 0 & 0 & \bar{u}_1 \end{pmatrix}, \ \mathbf{A}_2 = \begin{pmatrix} \bar{u}_2 & 0 & 0 & 0 & 0 \\ 0 & \bar{u}_2 & 0 & 0 & \bar{\zeta} \\ 0 & 0 & \bar{u}_2 & 0 & 0 \\ 0 & -\bar{\zeta} & 0 & \bar{u}_2 & 0 \\ 0 & \gamma\bar{p} & 0 & 0 & \bar{u}_2 \end{pmatrix}, \tag{3}$$

$$\mathbf{A}_3 = \begin{pmatrix} \bar{u}_3 & 0 & 0 & 0 & 0 \\ 0 & \bar{u}_3 & 0 & 0 & 0 \\ 0 & 0 & \bar{u}_3 & 0 & \bar{\zeta} \\ 0 & 0 & -\bar{\zeta} & \bar{u}_3 & 0 \\ 0 & 0 & \gamma\bar{p} & 0 & \bar{u}_3 \end{pmatrix}, \ \mathbf{C} = \begin{pmatrix} \frac{\partial \bar{u}_1}{\partial x_1} & \frac{\partial \bar{u}_1}{\partial x_2} & \frac{\partial \bar{u}_1}{\partial x_3} & \frac{\partial \bar{p}}{\partial x_1} & 0 \\ \frac{\partial \bar{u}_2}{\partial x_1} & \frac{\partial \bar{u}_2}{\partial x_2} & \frac{\partial \bar{u}_2}{\partial x_3} & \frac{\partial \bar{p}}{\partial x_2} & 0 \\ \frac{\partial \bar{u}_3}{\partial x_1} & \frac{\partial \bar{u}_3}{\partial x_2} & \frac{\partial \bar{u}_3}{\partial x_3} & \frac{\partial \bar{p}}{\partial x_3} & 0 \\ \frac{\partial \bar{\zeta}}{\partial x_1} & \frac{\partial \bar{\zeta}}{\partial x_2} & \frac{\partial \bar{\zeta}}{\partial x_3} & -\nabla\cdot\bar{\mathbf{u}} & 0 \\ \frac{\partial \bar{p}}{\partial x_1} & \frac{\partial \bar{p}}{\partial x_2} & \frac{\partial \bar{p}}{\partial x_3} & 0 & \gamma\nabla\cdot\bar{\mathbf{u}} \end{pmatrix}. \tag{4}$$

Note that the $\{\mathbf{A}_i : i = 1,2,3\}$ matrices are functions of the base flow vector $\bar{\mathbf{q}}$; the matrix $\mathbf{C}$ is a function of $\nabla\bar{\mathbf{q}}$. Note also that all the matrices (3)–(4) are independent of time, as the mean flow $\bar{\mathbf{q}}$ is assumed to be steady. In the case of uniform base flow, $\nabla\bar{\mathbf{q}} \equiv \mathbf{0}$, so that $\frac{\partial \mathbf{A}_i}{\partial x_j} \equiv \mathbf{0}$ for $i, j = 1,2,3$, and $\mathbf{C} \equiv \mathbf{0}$. The symbol γ denotes the ratio of specific heats: $\gamma = c_p/c_v$.

DOI: 10.1002/nme

It is a well-known fact that the system (2) is hyperbolic [29]. This implies that the tensor $\mathbf{A}_n \equiv \mathbf{A}_1 n_1 + \mathbf{A}_2 n_2 + \mathbf{A}_3 n_3$, for some spatial orientation $\mathbf{n}^{\mathrm{T}} = (n_1, \ n_2, \ n_3)$, is diagonalizable: $\mathbf{A}_n = \mathbf{S}\boldsymbol{\Lambda}_n\mathbf{S}^{-1}$. Here, $\mathbf{S}$ is the matrix that diagonalizes $\mathbf{A}_n$, and $\boldsymbol{\Lambda}_n$ is a diagonal matrix containing the eigenvalues of $\mathbf{A}_n$ (also referred to as the characteristic speeds):

$$\boldsymbol{\Lambda}_n = \begin{pmatrix} \bar{u}_n & & & & & \\ & \bar{u}_n & & & & \\ & & \bar{u}_n & & & \\ & & & \bar{u}_n + \bar{c} & & \\ & & & & \bar{u}_n - \bar{c} & \end{pmatrix}, \tag{5}$$

with $\bar{c} = \sqrt{\gamma \bar{p} \bar{\xi}}$ denoting the speed of sound. Defining $\mathbf{v}' \equiv \mathbf{S}^{-1}\mathbf{q}'$, the linearized Euler equations (2) in these so-called 'characteristic' variables are

$$\frac{\partial \mathbf{v}'}{\partial t} + \mathbf{S}^{-1}\mathbf{A}_i\mathbf{S}\frac{\partial \mathbf{v}'}{\partial x_i} + \mathbf{S}^{-1}\left[\mathbf{A}_i\frac{\partial \mathbf{S}}{d x_i} + \mathbf{C}\mathbf{S}\right]\mathbf{v}' = \mathbf{0}. \tag{6}$$

The characteristic variables are introduced here for the sake of applying the boundary conditions, which will be posed in the characteristic variables $\mathbf{v}'$ rather than the primitive variables $\mathbf{q}'$ (Section 4.1). Expressions for the diagonalizing matrix $\mathbf{S}$ and its inverse $\mathbf{S}^{-1}$ are given in Section A.1 of the Appendix. The reader may verify that, given the diagonalizing matrix $\mathbf{S}^{-1}$ (A.1), the characteristic variables vector is

$$\mathbf{v}' \equiv \begin{pmatrix} v_1' \\ v_2' \\ v_3' \\ v_4' \\ v_5' \end{pmatrix} = \begin{pmatrix} (n_3 v' - n_2 w' + n_1 \zeta') + \frac{\bar{\xi}}{\gamma \bar{p}} n_1 p' \\ (n_3 u' - n_1 w' - n_2 \zeta') - \frac{\bar{\xi}}{\gamma \bar{p}} n_2 p' \\ (n_2 u' - n_1 v' + n_3 \zeta') + \frac{\bar{\xi}}{\gamma \bar{p}} n_3 p' \\ \mathbf{u}_n' + \frac{\bar{c}}{\gamma \bar{p}} p' \\ -\mathbf{u}_n' + \frac{\bar{c}}{\gamma \bar{p}} p' \end{pmatrix}, \tag{7}$$

where $\mathbf{u}_n' \equiv \mathbf{u}' \cdot \mathbf{n}$. Note that, for the specific case of a uniform base flow, the equations (6) reduce to

$$\frac{\partial \mathbf{v}'}{\partial t} + \mathbf{S}^{-1}\mathbf{A}_i\mathbf{S}\frac{\partial \mathbf{v}'}{\partial x_i} = \mathbf{0}. \tag{8}$$

2.2. Overview of the Proper Orthogonal Decomposition/Galerkin approach for model reduction

The fluid ROM is built via the POD/Galerkin approach, reviewed succinctly here. For a detailed discussion of the POD/Galerkin approach applied to the Equation (2), the reader is referred to [18, 19].

The first step of the model reduction procedure is the calculation of a reduced basis using the POD of an ensemble of flow-field realizations. Discussed in detail in Lumley [33] and Holmes *et al.* [1], POD is a mathematical procedure that, given an ensemble of data and an inner product, denoted generically (for now) by $(\cdot, \cdot)$, constructs a basis for that ensemble that is optimal in the sense that it describes more energy (on average) of the ensemble in the chosen inner product than any other linear basis of the same dimension M. In the present context, the ensemble $\{\mathbf{u}^k(\mathbf{x}) : k = 1, \ldots, N\}$ is a set of N instantaneous snapshots of a CFD numerical solution field. It is a well-known result [1, 18, 34, 35] that the solution to the POD optimization problem reduces to the eigenvalue problem $\mathscr{R}\boldsymbol{\phi} = \lambda\boldsymbol{\phi}$, where $\mathscr{R} \equiv \langle \mathbf{u}^k \otimes \mathbf{u}^k \rangle$ is a self-adjoint and positive semidefinite operator. If it is assumed that $\mathscr{R}$ is compact, then there exists a countable set of non-negative eigenvalues λ_i with associated eigenfunctions $\boldsymbol{\phi}_i$. It can be shown [1, 33] that the set of M eigenfunctions, or POD modes, $\{\boldsymbol{\phi}_i : i = 1, \ldots, M\}$ corresponding to the M largest eigenvalues of $\mathscr{R}$ is precisely the desired basis.

DOI: 10.1002/nme

Given this basis, the numerical ROM solution $\mathbf{u}_M$ can be represented as a linear combination of POD modes

$$\mathbf{u}_M(\mathbf{x},t) = \sum_{j=1}^{M} a_j(t)\boldsymbol{\phi}_j(\mathbf{x}), \tag{9}$$

where the $a_j(t)$ are the so-called ROM coefficients, or modal amplitudes, to be solved for in the ROM.

The second step of the model reduction procedure is the projection of the governing system of PDEs onto the POD basis $\{\boldsymbol{\phi}_i\}$ in the inner product $(\cdot,\cdot)$. In this step, the full system dynamics are effectively translated to the implied dynamics of the POD modes. Suppose, for concreteness, that the governing system of equations for the state vector $\mathbf{u}$ has the form

$$\frac{\partial \mathbf{u}}{\partial t} = \mathscr{L}\mathbf{u} + \mathscr{N}_2(\mathbf{u},\mathbf{u}) + \mathscr{N}_3(\mathbf{u},\mathbf{u},\mathbf{u}), \tag{10}$$

where $\mathscr{L}$ is a linear differential operator, and $\mathscr{N}_2$ and $\mathscr{N}_3$ are quadratic and cubic operators, respectively. The Galerkin projection of (10) onto the POD mode $\boldsymbol{\phi}_j$ for $j = 1, 2, ..., M$ is

$$\left(\boldsymbol{\phi}_j, \frac{\partial \mathbf{u}_M}{\partial t}\right) = (\boldsymbol{\phi}_j, \mathscr{L}\mathbf{u}_M) + \left(\boldsymbol{\phi}_j, \mathscr{N}_2(\mathbf{u}_M,\mathbf{u}_M)\right) + \left(\boldsymbol{\phi}_j, \mathscr{N}_3(\mathbf{u}_M,\mathbf{u}_M,\mathbf{u}_M)\right). \tag{11}$$

Substituting the POD decomposition of $\mathbf{u}_M$ (9) into (11) and applying the orthonormality property of the basis functions $\boldsymbol{\phi}_i$ in the inner product $(\cdot,\cdot)$ gives a set of time-dependent ordinary differential equations (ODEs) for the modal amplitudes that accurately describes the flow dynamics of the full system of PDEs for some limited set of flow conditions:

$$\begin{aligned}\dot{a}_j \equiv \frac{\mathrm{d}a}{\mathrm{d}t} = &\sum\nolimits_{l=1}^{M} a_l(\boldsymbol{\phi}_j, \mathscr{L}(\boldsymbol{\phi}_l)) + \sum\nolimits_{l=1}^{M}\sum\nolimits_{m=1}^{M} a_l a_m(\boldsymbol{\phi}_j, \mathscr{N}_2(\boldsymbol{\phi}_l,\boldsymbol{\phi}_m)) \\ &+ \sum\nolimits_{l=1}^{M}\sum\nolimits_{m=1}^{M}\sum\nolimits_{n=1}^{M} a_l a_m a_n(\boldsymbol{\phi}_j, \mathscr{N}_3(\boldsymbol{\phi}_l,\boldsymbol{\phi}_m,\boldsymbol{\phi}_n)),\end{aligned} \tag{12}$$

for $j = 1, 2, \ldots, M$. The system (10) was chosen to have a cubic nonlinearity simply for the sake of demonstrating the projection step of the model reduction on a concrete example. Attention in the present work is restricted to linear systems, so that $\mathscr{N}_2 = \mathscr{N}_3 = \emptyset$ in (10)–(12).

2.3. Symmetry inner product and Galerkin projection of the governing fluid equations

In a POD/Galerkin ROM, the inner product is also a mathematical expression for the energy in the ROM. For the incompressible Navier–Stokes equations, the natural choice of inner product is the $L^2(\Omega)$ inner product, as the solution vector is taken to be the velocity vector $\mathbf{u}$, so that $||\mathbf{u}||_{L^2(\Omega)}$ is a measure of the global kinetic energy in the domain Ω. The $L^2(\Omega)$ inner product is therefore physically sensible for the incompressible Navier–Stokes equations: the POD modes optimally represent the kinetic energy present in the ensemble from which they are generated. The same is *not* true for the compressible linearized Euler equations (2) with solution vector $\mathbf{q}'$ as defined in Section 2.1. This fact is discussed at length in [18, 36], where it is demonstrated on several test cases that the $L^2(\Omega)$ inner product for these equations does not correspond to an energy integral, meaning if it is selected as the inner product defining the projection, the ROM solution does not satisfy the energy conservation relation implied by the governing equations.

DOI: 10.1002/nme

To define an appropriate inner product for the Galerkin projection of (2), some fundamental mathematical properties of this hyperbolic system are exploited. A key property of the hyperbolic system (2) is that it is symmetrizable,[‡] that is, there exists a symmetric, positive definite matrix $\mathbf{H}$ such that $\{\mathbf{HA}_i : i = 1, 2, 3\}$ are all symmetric. The symmetrizer of (2) is given by [18, 19]

$$\mathbf{H} = \begin{pmatrix} \bar{\rho} & 0 & 0 & 0 & 0 \\ 0 & \bar{\rho} & 0 & 0 & 0 \\ 0 & 0 & \bar{\rho} & 0 & 0 \\ 0 & 0 & 0 & \alpha^2\gamma\bar{\rho}^2\bar{p} & \bar{\rho}\alpha^2 \\ 0 & 0 & 0 & \bar{\rho}\alpha^2 & \frac{(1+\alpha^2)}{\gamma\bar{p}} \end{pmatrix}, \tag{13}$$

where α is an arbitrary real, nonzero parameter. Pre-multiplying (2) by the matrix $\mathbf{H}$ yields the following symmetrized system:

$$\frac{\partial(\mathbf{Hq}')}{\partial t} + \mathbf{HA}_i \frac{\partial \mathbf{q}'}{\partial x_i} + \mathbf{HCq}' = \mathbf{0}. \tag{14}$$

As will be proven formally in Lemma 4.3.1, an appropriate choice of inner product for the system (2) is the so-called 'symmetry inner product' defined as

$$(\mathbf{q}'^{(1)}, \mathbf{q}'^{(2)})_{(\mathbf{H},\Omega)} \equiv \int_\Omega \mathbf{q}'^{(1)} \mathbf{H} \mathbf{q}'^{(2)} d\Omega. \tag{15}$$

Given $\mathbf{H}$ (13), the expression for the symmetry inner product with respect to $\mathbf{H}$ over Ω is

$$\begin{aligned}(\mathbf{q}'^{(1)}, \mathbf{q}'^{(2)})_{(\mathbf{H},\Omega)} = \int_\Omega \Big[&\bar{\rho}\mathbf{u}'^{(1)} \cdot \mathbf{u}'^{(2)} + \alpha^2\gamma\bar{\rho}^2\zeta'^{(1)}\zeta'^{(2)} + \frac{1+\alpha^2}{\gamma\bar{p}} p'^{(1)} p'^{(2)} \\ &+ \alpha^2\bar{\rho}(\zeta'^{(2)} p'^{(1)} + \zeta'^{(1)} p'^{(2)}) \Big] \, d\Omega.\end{aligned} \tag{16}$$

Equation (15) defines a valid inner product because $\mathbf{H}$ is symmetric positive definite. Expanded in its modal basis, the ROM solution $\mathbf{q}'_M$ is expressed as

$$\mathbf{q}'_M(\mathbf{x}, t) = \sum_{k=1}^{M} a_k(t) \boldsymbol{\phi}_k(\mathbf{x}). \tag{17}$$

The components of the five-vector $\boldsymbol{\phi}_k$ are denoted ϕ_k^i for $i = 1, \ldots, 5$, that is

$$\boldsymbol{\phi}_k^{\mathrm{T}} = \begin{pmatrix} \phi_k^1, & \phi_k^2, & \phi_k^3, & \phi_k^4, & \phi_k^5 \end{pmatrix}. \tag{18}$$

The Galerkin projection of the system of Equation (2) onto the j^{th} mode, for $j = 1, \ldots, M$, in the $(\mathbf{H}, \Omega)$ inner product is

$$\left(\boldsymbol{\phi}_j, \frac{\partial \mathbf{q}'_M}{\partial t}\right)_{(\mathbf{H},\Omega)} + \left(\boldsymbol{\phi}_j, \mathbf{A}_i \frac{\partial \mathbf{q}'_M}{\partial x_i}\right)_{(\mathbf{H},\Omega)} + (\boldsymbol{\phi}_j, \mathbf{C}\mathbf{q}'_M)_{(\mathbf{H},\Omega)} = 0. \tag{19}$$

Equation (19) gives rise to the following set of M linear ODEs for the time-dependent ROM coefficients $\{a_j(t) : j = 1, 2, \ldots, M\}$:

$$\dot{a}_j(t) = -\sum_{k=1}^{M} a_k(t) \left(\boldsymbol{\phi}_j, \mathbf{A}_i \frac{\partial \boldsymbol{\phi}_k}{\partial x_i}\right)_{(\mathbf{H},\Omega)} - \sum_{k=1}^{M} a_k(t) (\boldsymbol{\phi}_j, \mathbf{C}\boldsymbol{\phi}_k)_{(\mathbf{H},\Omega)}, \tag{20}$$

where $\dot{a}_j(t) \equiv \frac{\partial a_j}{\partial t}$.

[‡]Among other hyperbolic systems of interest that are symmetrizable are the nonlinear Euler equations [37], the compressible Navier–Stokes equations [38], and the shallow water equations [39]. Most hyperbolic systems derived from conservation laws can be symmetrized ([40, Chapter 6]). A (non-unique) symmetrizer of a matrix (or set of matrices) can be derived using the eigenvectors of the matrix (or matrices), following techniques presented by Gustafsson in [29, 31]. Other symmetric forms of both the linearized Euler and linearized Navier–Stokes equations can be found in Oliger and Sundstrom [32] and in Abarbanel and Gottlieb [41].

DOI: 10.1002/nme

The equations (2) and the reduced system (20) are posed on an open-bounded domain $\Omega \subset \mathbb{R}^3$ with boundary $\partial\Omega$. In the FSI problem considered here, $\partial\Omega$ will include the boundary of the structure or plate that lies in the fluid domain defined in (22). Discussion of the boundary conditions is deferred until Section 4.1.

3. STRUCTURE REDUCED ORDER MODEL OF LINEARIZED VON KÁRMÁN PLATE

The von Kármán plates are a class of nonlinear plates that takes into account in-plane stretching. With the Kirchhoff assumption [42], the equations of motion for a thin plate with a membrane nonlinearity and thickness h take the form [43, 44]

$$\begin{aligned}\rho_s h w_{,tt} + \mathscr{D}\nabla^4 w = g + \frac{12\mathscr{D}}{h^2}\Bigg[&\left(u_{,x} + \frac{1}{2}w_{,x}^2\right)(w_{,xx} + \nu w_{,yy}) + \left(v_{,y} + \frac{1}{2}w_{,y}^2\right)(w_{,yy} + \nu w_{,xx}) \\ &+(1-\nu)(u_{,y} + v_{,x} + w_{,x}w_{,y})w_{,xy}\Bigg], \\ u_{,xx} + w_{,x}w_{,xx} + \frac{1}{2}(1-\nu)(u_{,yy} + w_{,x}w_{,yy}) + \frac{1}{2}(1+\nu)(v_{,xy} + w_{,y}w_{,xy}) &= 0, \\ v_{,yy} + w_{,y}w_{,yy} + \frac{1}{2}(1-\nu)(v_{,xx} + w_{,y}w_{,xx}) + \frac{1}{2}(1+\nu)(u_{,xy} + w_{,x}w_{,xy}) &= 0.\end{aligned} \tag{21}$$

Here, u, v, and w denote the x_1-, x_2-, and x_3- displacements of the plate, respectively, ρ_s is the linear density of the plate, $\mathscr{D} \equiv \frac{Eh^3}{12(1-\nu^2)}$ with E denoting the elastic (Young's) modulus, ν is the Poisson ratio, and $g \equiv g(x_1, x_2, t)$ is an applied external load per unit length. A ROM for the full nonlinear von Kármán plate equations (21) was developed using the method of quadratic components and a Galerkin projection in [43, 44]. In the present work, attention is restricted to the special simplified case of the more general von Kármán equations (21), namely the linearized von Kármán equation for the x_3- displacement. This equation and the underlying assumptions are described in the following subsection.

3.1. Linearized von Kármán plate equation

Consider a thin, elastic, rectangular plate with dimensions $L_x \times L_y$, situated in the $x_3 = 0$ plane of the fluid domain Ω (Figure 1):

$$\partial\Omega \equiv \{(x_1, x_2) \in \mathbb{R}^2 : 0 \leqslant x_1 \leqslant L_x, 0 \leqslant x_2 \leqslant L_y\}. \tag{22}$$

The plate surface is denoted with a $'\partial'$ because the surface of the plate represents the two-dimensional boundary of the domain Ω in which the fluid equations (2) are posed. x_1 is the direction of the fluid flow; x_2 is the in-plane direction orthogonal to the flow. Assuming the plate undergoes small deformations restricted to the direction normal to the plate, which leads to the out-of-plane (or x_3-direction) displacement field $w(x_1, x_2, t)$, equation (21) simplify to the linear plate equation

$$\rho_s h w_{,tt} + \mathscr{D}\nabla^4 w = g. \tag{23}$$

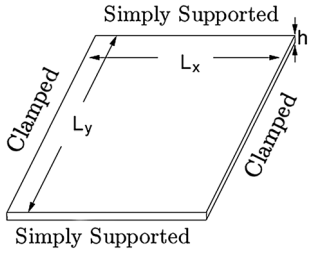

Figure 1. Geometry of the von Kármán plate problem.

DOI: 10.1002/nme

Equation (23) is also referred to as the Kirchhoff–Love plate model. The scenario considered in the present work is illustrated in Figure 1. The fore and aft boundaries of the plate are clamped (24), whereas the side boundaries are simply supported (25).

Mathematically, this scenario is expressed as the following boundary conditions:

$$w(0,x_2,t)=0=w(L_x,x_2,t),\quad \frac{\partial w}{\partial x_1}(0,x_2,t)=0=\frac{\partial w}{\partial x_1}(L_x,x_2,t). \tag{24}$$

$$w(x_1,0,t)=0=w(x_1,L_y,t),\quad \frac{\partial^2 w}{\partial x_2^2}(x_1,0,t)=0=\frac{\partial^2 w}{\partial x_2^2}(x_1,L_y,t). \tag{25}$$

The applied external load g is assumed to be free of shear components.

3.2. Galerkin model reduction of the linearized plate equation

The ROM for the linearized plate equation (23) is built using a Galerkin approximation [43, 44]. First, the out-of-plane (or x_3-) displacement, $w(x_1,x_2,t)$, is expanded in a scalar-reduced basis $\{\xi_k(x_1,x_2):k=1,2,\ldots,P\}$

$$w_P(x_1,x_2,t)=\sum_{i=1}^{P} b_i(t)\xi_i(x_1,x_2), \tag{26}$$

where P is the number of structure modes retained. The mode shapes $\xi_i(x,y)$ are taken to be the eigenmodes of the homogeneous variant of the linearized plate equation (23). These basis functions are orthonormal with respect to the mass matrix in the usual $L^2(\partial\Omega)$ inner product, so that

$$(\xi_i,\rho_s h\xi_j)_{L^2(\partial\Omega)}\equiv\int_{\partial\Omega}\rho_s h\xi_i\xi_j\,\mathrm{d}S=\int_0^{L_x}\int_0^{L_y}\rho_s h\xi_i\xi_j\,\mathrm{d}x_2\mathrm{d}x_1=\delta_{ij}, \tag{27}$$

where δ_{ij} denotes the Krönecker delta function. In (26), the coefficients $b_i(t)$ are the unknown, time-dependent DoFs to be solved for in solving the ROM. Substituting the expansion (26) into (23), projecting the resulting system onto the kth mode ξ_k in the L^2 inner product and invoking the orthonormality of the ξ_k, the following set of equations is obtained:

$$\ddot{b}_k(t)+\mathscr{D}\sum_{l=1}^{P} b_l(t)\left(\nabla^4\xi_l,\xi_k\right)_{L^2(\partial\Omega)}=(g,\xi_k)_{L^2(\partial\Omega)}, \tag{28}$$

for $k=1,\ldots,P$, where $\ddot{b}_k\equiv\frac{\partial^2 b_k}{\partial t^2}$.

It is well known [45] that, for any linear rectangular plate with homogeneous boundary conditions, the functions $\nabla^4\xi_k$ and ξ_j are orthogonal in the $L^2(\partial\Omega)$ inner product, that is,

$$\left(\nabla^4\xi_k,\xi_j\right)_{L^2(\partial\Omega)}=0\ \text{ for }\ k\neq j. \tag{29}$$

Applying this identity, the following is obtained:

$$\ddot{b}_k+\omega_k^2 b_k=G_k(t), \tag{30}$$

where

$$\omega_k^2\equiv\mathscr{D}(\nabla^4\xi_k,\xi_k)_{L^2(\partial\Omega)}, \tag{31}$$

$$G_k(t)\equiv(g,\xi_k)_{L^2(\partial\Omega)}, \tag{32}$$

for $k=1,\ldots,P$. Equation (30) is the structure ROM dynamical system for the structure modal amplitudes $\{b_k:k=1,\ldots,P\}$, analogous to the fluid modal system (20). Physically, the ω_k (31) represents the natural frequencies of the plate.

DOI: 10.1002/nme

4. NUMERICAL STABILITY OF COUPLED LINEARIZED FLUID/STRUCTURE SYSTEM

4.1. Coupling of structure and fluid reduced order models via boundary conditions

The fluid and structure ROMs are coupled through the external load $g(x_1, x_2, t)$, applied on the plate $\partial\Omega$, as well as through the boundary conditions on the fluid variables on $\partial\Omega$. Because it is assumed that the applied fluid loading on the plate is free of shear components, the external load $g(x_1, x_2, t)$ on the right-hand side of (23) consists of the static pressure only. This physical assumption is expressed mathematically as

$$g(x_1, x_2, t) = -p'(x_1, x_2, 0, t) \quad \text{on} \quad \partial\Omega, \tag{33}$$

where $p'(x_1, x_2, 0, t)$ is the fluid pressure on the plate $\partial\Omega$ (22). The pressure is applied downward, and g is taken as positive when acting in the positive x_3- direction.

The pressure (33) represents one side of the coupling of the fluid and structure. Additional coupling terms arise from the boundary conditions on the fluid variables at the plate boundary. Given the chosen (inviscid) fluid equations, the natural choice of boundary condition at the solid wall boundary is a linearized version of the no-penetration boundary condition,[§] $\mathbf{u} \cdot \mathbf{n} = -\dot{w}$:

$$u'_n = -\bar{\mathbf{u}} \cdot \nabla w - \dot{w} \equiv u'_p \quad \text{on} \quad \partial\Omega. \tag{34}$$

Here, w and $\dot{w}$ are respectively the solid wall displacement and velocity in the $-\mathbf{n}$ direction, with $\mathbf{n}$ denoting the outward unit normal to the solid wall boundary $\partial\Omega$ and $u'_n \equiv \mathbf{u}' \cdot \mathbf{n}$.

In practical applications, the FSI initial boundary value problem (IBVP) is likely to be posed on an infinite or semi-infinite domain. In this case, the boundary is decomposed as $\partial\Omega \equiv \partial\Omega_P \cup \partial\Omega_F$, with $\partial\Omega_P$ denoting the plate boundary (22) and $\partial\Omega_F$ denoting the far-field boundary [18, 19], and an appropriate boundary condition is imposed at the far-field. An appropriate far-field boundary condition, termed the non-reflecting boundary condition, is one that will suppress the reflection of waves from the outer computational boundaries. All outgoing unsteady characteristic waves are allowed to exit the flow domain at the far-field boundary without reflection, that is, without being allowed to re-enter the domain through the boundary. This is accomplished by setting the components of $\mathbf{v}'$ corresponding to characteristic waves traveling into Ω (those corresponding to negative eigenvalues of $\mathbf{A}_n$) to zero. It is shown in [18, 19] that the non-reflecting far-field boundary condition is, by construction, well-posed and stable for the governing fluid equations. Attention may therefore be restricted, without loss of generality, to the condition that couples the fluid and structure ROMs, namely the condition at the plate (34).

4.2. Implementation of plate boundary conditions

The linearized no-penetration condition (34) is posed in the characteristic variables $\mathbf{v}'$ (6) as an acoustically reflecting condition. Assuming the base flow satisfies a no-penetration condition at the plate ($\bar{u}_n \equiv 0$ on $\partial\Omega$), the characteristic speeds are $\{0, 0, 0, \bar{c}, -\bar{c}\}$. In particular, the fourth characteristic is outgoing and the fifth characteristic is incoming. For a stationary plate, specifying the acoustically reflecting boundary condition amounts to setting the incoming characteristic, v'_5, equal to the outgoing characteristic, v'_4. From (7), the reader may observe that $v'_4 = \mathbf{u}'_n + \frac{\bar{c}}{\gamma\bar{p}}$ and $v'_5 = -\mathbf{u}'_n + \frac{\bar{c}}{\gamma\bar{p}}$. Thus, when the plate velocity is $u'_p \equiv u'_p(x_1, x_2, t)$, the following relation satisfies (34)

$$v'_5 = v'_4 - 2u'_p \quad \text{on} \quad \partial\Omega. \tag{35}$$

[§]The no-penetration boundary condition is derived by requiring that the material derivative of the bounding surface $F(x, y, z, t) = 0$ vanish on the surface, that is, $\frac{DF}{Dt} = \frac{\partial F}{\partial t} + \mathbf{u} \cdot \nabla F = 0$. Substituting $F = w(x, y, z, t) - z$ and $\mathbf{u} = \bar{\mathbf{u}} + \mathbf{u}'$, and linearizing the resulting expression leads to (34). See [46] for a more detailed discussion.

DOI: 10.1002/nme

The condition (35) is equivalent to substituting

$$\mathbf{v}' \leftarrow \mathbf{v}'_p \equiv \begin{pmatrix} v'_1 \\ v'_2 \\ v'_3 \\ v'_4 \\ v'_4 - 2u'_p \end{pmatrix} \quad \text{on} \quad \partial\Omega. \tag{36}$$

The boundary condition (36) for the fluid ROM can be implemented efficiently using a weak formulation. The system of PDEs (2) is projected onto the jth POD mode in the $(\mathbf{H}, \Omega)$ inner product, as in (19). The second term in (19) is integrated by parts, and the vector specifying the boundary condition is inserted into the boundary integral over $\partial\Omega$ that arises

$$\left(\boldsymbol{\phi}_j, \frac{\partial \mathbf{q}'_M}{\partial t}\right)_{(\mathbf{H},\Omega)} = -\int_{\partial\Omega} \boldsymbol{\phi}_j^{\mathrm{T}} \mathbf{H} \mathbf{A}_n \mathbf{q}'_p \, \mathrm{d}S + \int_\Omega \left[\frac{\partial}{\partial x_i}\left[\boldsymbol{\phi}_j^{\mathrm{T}} \mathbf{H} \mathbf{A}_i\right] - \boldsymbol{\phi}_j^{\mathrm{T}} \mathbf{H} \mathbf{C}\right] \mathbf{q}'_M \, \mathrm{d}\Omega. \tag{37}$$

Performing an additional integration by parts on the first term in the volume integral in (37) yields

$$\int_\Omega \frac{\partial}{\partial x_i}\left[\boldsymbol{\phi}_j^{\mathrm{T}} \mathbf{H} \mathbf{A}_i\right] \mathbf{q}'_M \, \mathrm{d}\Omega = \int_{\partial\Omega} \boldsymbol{\phi}_j^{\mathrm{T}} \mathbf{H} \mathbf{A}_n \mathbf{q}'_M \, \mathrm{d}S - \int_\Omega \boldsymbol{\phi}_j^{\mathrm{T}} \mathbf{H} \mathbf{A}_i \frac{\partial \mathbf{q}'_M}{\partial x_i} \, \mathrm{d}\Omega, \tag{38}$$

so that (37) is equivalent to

$$\left(\boldsymbol{\phi}_j, \frac{\partial \mathbf{q}'_M}{\partial t}\right)_{(\mathbf{H},\Omega)} = -\left(\boldsymbol{\phi}_j, \mathbf{A}_i \frac{\partial \mathbf{q}'_M}{\partial x_i} + \mathbf{C}\mathbf{q}'_M\right)_{(\mathbf{H},\Omega)} + \int_{\partial\Omega} \boldsymbol{\phi}_j^{\mathrm{T}} \mathbf{H} \mathbf{A}_n (\mathbf{q}'_M - \mathbf{q}'_p) \, \mathrm{d}S. \tag{39}$$

The solid wall boundary condition is implemented by substituting the vector $\mathbf{q}'_p \equiv \mathbf{S}\mathbf{v}'_p$, where $\mathbf{v}'_p$ is as in (36), into the boundary integral that appears in (39). After some careful algebraic manipulations, it can be shown that the first integrand that appears in (37) is

$$\boldsymbol{\phi}_j^{\mathrm{T}} \mathbf{H} \mathbf{A}_n \mathbf{q}'_p = \underbrace{\bar{\rho}\bar{c}\phi_j^n (u'_{n,M} - u'_p)}_{\text{penalty-like term}} + \underbrace{\phi_j^n p'_M + \phi_j^5 u'_p}_{=\boldsymbol{\phi}_j^{\mathrm{T}} \mathbf{H} \mathbf{A}_n \mathbf{q}'_M}, \tag{40}$$

where $\phi_j^n \equiv \phi_j^1 n_1 + \phi_j^2 n_2 + \phi_j^3 n_3$. The first term in (40) can be viewed as a penalty term that forces the normal velocity to the prescribed boundary value. In a coupled ROM such as the one considered herein, the velocity u'_p is given by (34), so that

$$\boldsymbol{\phi}_j^{\mathrm{T}} \mathbf{H} \mathbf{A}_n (\mathbf{q}'_M - \mathbf{q}'_p) = -\bar{\rho}\bar{c}\phi_j^n (u'_{n,M} - u'_p) = -\bar{\rho}\bar{c}\phi_j^n \left(u'_{n,M} + \dot{w} + \bar{u}\frac{\partial w}{\partial x_1}\right), \tag{41}$$

because $\bar{\mathbf{u}} \cdot \nabla w = \bar{u}\frac{\partial w}{\partial x_1}$ on the surface of the plate. By substituting the modal decompositions (9) and (26) into (41), (39) becomes a linear system of ODEs, namely:

$$\begin{aligned} \dot{a}_j = &-\sum_{k=1}^{M} a_k \left[\left(\boldsymbol{\phi}_j, \mathbf{A}_i \frac{\partial \phi_k}{\partial x_i} + \mathbf{C}\phi_k\right)_{(\mathbf{H},\Omega)} + \int_{\partial\Omega} \bar{\rho}\bar{c}\phi_j^n \phi_k^n \mathrm{d}S\right] \\ &- \sum_{k=1}^{P} b_k \int_{\partial\Omega} \bar{\rho}\bar{c}\bar{u}\phi_j^n \frac{\partial \xi_k}{\partial x_1} \, \mathrm{d}S - \sum_{k=1}^{P} \dot{b}_k \int_{\partial\Omega} \bar{\rho}\bar{c}\phi_j^n \xi_k \, \mathrm{d}S, \end{aligned} \tag{42}$$

for $j = 1, \ldots, M$. Now, expanding the right-hand side of (33) in terms of $\phi^5(\mathbf{x})$, the fifth component of the fluid ROM basis, this expression becomes

$$g(x_1, x_2, t) = -\sum_{i=1}^{M} a_i(t)\phi_i^5(x_1, x_2, 0), \tag{43}$$

on the plate $\partial\Omega$, so that (30) simplifies to

$$\ddot{b}_k = -\mathscr{D} b_k \int_{\partial\Omega} \nabla^4 \xi_k \xi_k \mathrm{d}S - \sum_{i=1}^{M} a_i \int_{\partial\Omega} \phi_i^5 \xi_k \mathrm{d}S, \tag{44}$$

for $k = 1, \ldots, P$.

DOI: 10.1002/nme

It is straightforward to see that (42) along with (44) define an $(M + 2P) \times (M + 2P)$ linear system of the form

$$\begin{pmatrix} \dot{\mathbf{f}} \\ \dot{\mathbf{s}} \end{pmatrix} = \begin{pmatrix} \mathbf{A} & \mathbf{B} \\ \mathbf{C} & \mathbf{D} \end{pmatrix} \begin{pmatrix} \mathbf{f} \\ \mathbf{s} \end{pmatrix}, \tag{45}$$

where

$$\mathbf{s}^{\mathrm{T}} \equiv \begin{pmatrix} b_1(t), & \cdots, & b_P(t), & \dot{b}_1(t), & \cdots, & \dot{b}_P(t) \end{pmatrix} \in \mathbb{R}^{2P}, \tag{46}$$

$$\mathbf{f}^{\mathrm{T}} \equiv \begin{pmatrix} a_1(t), & \cdots, & a_M(t) \end{pmatrix} \in \mathbb{R}^{M}, \tag{47}$$

with P and M denoting the number of structure and fluid modes, respectively. Equation (45) is the coupled fluid and structure ROM, to be solved for the structure modal amplitudes $b_k(t)$ and fluid modal amplitudes $a_k(t)$. This is performed by advancing (45) forward in time using a fourth-order implicit Runge–Kutta scheme. The entries of the submatrices that appear in (45) can be inferred from (42) and (44), and are given in Section A.2 of the Appendix. The coupling matrices **B** and **C** arise because of the boundary conditions on the plate $\partial\Omega$.

4.3. Numerical stability of the coupled fluid–structure interaction reduced order model

The main result of this section is Theorem 4.3.3, which shows numerical stability of the coupled fluid/structure linear system (45) if a perturbed pressure loading of the form $g = -p' + \mathscr{O}\left(u'_{n,M} - u'_p\right)$ is applied on the plate – that is, a pressure loading 'stabilized' by a stabilization term of the form $K\left(u'_{n,M} - u'_p\right)$ for some constant $K \in \mathbb{R}$. Before studying the stability of the coupled system (45), stability of the fluid-only and structure-only systems, $\dot{\mathbf{f}} = \mathbf{A}\mathbf{f}$ and $\dot{\mathbf{s}} = \mathbf{C}\mathbf{s}$, respectively, must be shown. A sufficient condition for a Galerkin scheme to be stable in some inner product is that the energy associated with this projection in the selected inner product is non-increasing (Section A.3 of the Appendix).

Lemma 4.3.1
Assume the base flow field satisfies a no-penetration condition on the plate ($\bar{u}_n = 0$) and the base flow is uniform ($\nabla\bar{\mathbf{q}} = \mathbf{0}$). Then the Galerkin projection of the linearized compressible Euler equations (2) in the symmetry inner product $(\mathbf{H}, \Omega)$ with the linearized acoustically reflecting boundary condition (34) is stable for the fluid ROM, with energy estimate

$$\frac{\mathrm{d}E_f}{\mathrm{d}t} \equiv \frac{1}{2}\frac{\mathrm{d}}{\mathrm{d}t}||\mathbf{q}'_M||^2_{(\mathbf{H},\Omega)} \leqslant 0, \tag{48}$$

where $\mathbf{q}'_M$ is given by (17). That is, the discrete fluid-only ROM system $\dot{\mathbf{f}} = \mathbf{A}\mathbf{f}$ is stable.

Proof
Let the energy associated with the Galerkin projection of the fluid-only ROM $\dot{\mathbf{f}} = \mathbf{A}\mathbf{f}$ be defined by

$$E_f \equiv \frac{1}{2}||\mathbf{q}'_M||^2_{(\mathbf{H},\Omega)}, \tag{49}$$

where $\mathbf{q}'_M \equiv \sum_{k=1}^{M} a_k(t)\boldsymbol{\phi}_k(\mathbf{x})$ is the Galerkin approximation to the fluid solution. If the base flow is assumed to be uniform, the matrix **C** in (2) is identically zero. Then, from (2) and upon

DOI: 10.1002/nme

substitution of the acoustically reflecting boundary condition (34) on $\partial\Omega$:

$$\begin{aligned}
\frac{1}{2}\frac{\mathrm{d}}{\mathrm{d}t}||\mathbf{q}'_M||^2_{(\mathbf{H},\Omega)} &= \frac{1}{2}\frac{\mathrm{d}}{\mathrm{d}t}(\mathbf{q}'_M,\mathbf{q}'_M)_{(\mathbf{H},\Omega)} \\
&= \int_\Omega \mathbf{q}'^{\mathrm{T}}_M \mathbf{H}\frac{\partial \mathbf{q}'_M}{\partial t}\mathrm{d}\Omega \\
&= -\int_\Omega \mathbf{q}'^{\mathrm{T}}_M \mathbf{H}\mathbf{A}_i \frac{\partial \mathbf{q}'_M}{\partial x_i}\mathrm{d}\Omega \\
&= -\int_{\partial\Omega} \mathbf{q}'^{\mathrm{T}}_M \mathbf{H}\mathbf{A}_n \mathbf{q}'_p \mathrm{d}S + \frac{1}{2}\int_\Omega \frac{\partial}{\partial x_i}\left(\mathbf{q}'^{\mathrm{T}}_M \mathbf{H}\mathbf{A}_i \mathbf{q}'_M\right)\mathrm{d}\Omega \\
&\quad + \frac{1}{2}\int_\Omega \mathbf{q}'^{\mathrm{T}}_M \underbrace{\frac{\partial(\mathbf{H}\mathbf{A}_i)}{\partial x_i}}_{=\mathbf{0}\text{ (uniform base flow)}} \mathbf{q}'_M \mathrm{d}\Omega \\
&= -\int_{\partial\Omega} \mathbf{q}'^{\mathrm{T}}_M \mathbf{H}\mathbf{A}_n \mathbf{q}'_p \mathrm{d}S + \frac{1}{2}\int_{\partial\Omega} \mathbf{q}'^{\mathrm{T}}_M \mathbf{H}\mathbf{A}_n \mathbf{q}'_M \mathrm{d}S \\
&= \int_{\partial\Omega} \mathbf{q}'^{\mathrm{T}}_M \mathbf{H}\mathbf{A}_n \left(\frac{1}{2}\mathbf{q}'_M - \mathbf{q}'_p\right)\mathrm{d}S.
\end{aligned} \tag{50}$$

In going from line three to line four in (50), the property that the $\mathbf{H}\mathbf{A}_i$ for $i = 1, 2, 3$ are all symmetric has been invoked.

As discussed in Section 4.1, the acoustically reflecting boundary condition is expressed in the characteristic variables (36). In these variables, the integrand on the right-hand side of the last line of (50) is

$$\mathbf{q}'^{\mathrm{T}}_M \mathbf{H}\mathbf{A}_n \left(\frac{1}{2}\mathbf{q}'_M - \mathbf{q}'_p\right) = \frac{1}{2}\mathbf{q}'^{\mathrm{T}}_M \mathbf{H}\mathbf{A}_n \mathbf{q}'_M - \mathbf{q}'^{\mathrm{T}}_M \mathbf{H}\mathbf{S}\mathbf{\Lambda}_n \mathbf{v}'_p. \tag{51}$$

By substituting $\mathbf{q}'_p \leftarrow \mathbf{S}\mathbf{v}'_p$ with $\mathbf{v}'_p$ defined in (36) into the right-hand side of (51) and performing some careful algebraic manipulations, the following is obtained:

$$\mathbf{q}'^{\mathrm{T}}_M \mathbf{H}\mathbf{S}\mathbf{\Lambda}_n \mathbf{v}'_p = \bar{\rho}\bar{c}u'_{n,M}\left[u'_{n,M} - u'_p\right] + u'_{n,M}p'_M + u'_p p'_M. \tag{52}$$

Equation (52) employs the shorthand

$$u'_{n,M} \equiv \mathbf{u}'_M \cdot \mathbf{n}. \tag{53}$$

Further algebraic manipulations reveal that

$$\mathbf{q}'^{\mathrm{T}}_M \mathbf{H}\mathbf{A}_n \mathbf{q}'_M = 2p'_M u'_{n,M}, \tag{54}$$

so that

$$\begin{aligned}
\frac{1}{2}\mathbf{q}'^{\mathrm{T}}_M \mathbf{H}\mathbf{A}_n \mathbf{q}'_M - \mathbf{q}'^{\mathrm{T}}_M \mathbf{H}\mathbf{S}\mathbf{\Lambda}_n \mathbf{v}'_p &= -\bar{\rho}\bar{c}u'_{n,M}\left[u'_{n,M} - u'_p\right] - u'_p p'_M \\
&= -\bar{\rho}\bar{c}(u'_{n,M})^2 + \left(\bar{\rho}\bar{c}u'_{n,M} - p'_M\right)u'_p.
\end{aligned} \tag{55}$$

In the case that the fluid-only equations, u'_p is a given constant value. Then, according to the definition of stability (Section A.3 of the Appendix), it is sufficient to consider the homogeneous version of the boundary condition (34) ($u'_p = 0$) to show stability of the more general inhomogeneous boundary condition. Setting $u'_p = 0$ in (55) and substituting (51) into the last line of (50), the energy estimate

$$\frac{1}{2}\frac{\mathrm{d}}{\mathrm{d}t}||\mathbf{q}'_M||^2_{(\mathbf{H},\Omega)} = \int_{\partial\Omega} -\bar{\rho}\bar{c}(u'_{n,M})^2 \mathrm{d}S \leqslant 0, \tag{56}$$

is obtained.

DOI: 10.1002/nme

The physical implication of (56) is that the energy of the Galerkin projection of the linearized compressible Euler equations (2) in the $(\mathbf{H}, \Omega)$ inner product with the acoustically reflecting boundary condition (34) is non-increasing, a sufficient condition for numerical stability of the Galerkin scheme. □

Lemma 4.3.2
The Galerkin projection of the linearized von Kármán plate equation (23) for the out-of-plane (or x_3-) displacement of the plate in the $L^2(\partial\Omega)$ inner product is stable, with energy estimate

$$\frac{\mathrm{d}E_p}{\mathrm{d}t} \equiv \frac{1}{2}\frac{\mathrm{d}}{\mathrm{d}t}||\mathbf{r}'_P||^2_{L^2(\partial\Omega)} \leqslant 0, \tag{57}$$

where

$$\mathbf{r}_P \equiv \begin{pmatrix} w_P \\ \dot{w}_P \end{pmatrix}, \tag{58}$$

with w_P given by (26). That is, the discrete structure-only ROM system $\dot{\mathbf{s}} = \mathbf{D}\mathbf{s}$ is stable.

Proof
As in the proof of Lemma 4.3.1, it is sufficient to show stability for $g = 0$, which will imply stability for all $g \neq 0$ by Section A.3 of the Appendix. Setting the right-hand side of (23) to zero, the following is obtained:

$$\ddot{w}_P + \mathscr{D}(\nabla^4 w_P) = 0. \tag{59}$$

Equation (59) can be written as the following first-order system:

$$\dot{\mathbf{r}}_P + \underbrace{\begin{pmatrix} 0 & -1 \\ \mathscr{D}\nabla^4 & 0 \end{pmatrix}}_{\equiv \mathbf{G}} \mathbf{r}_P = 0. \tag{60}$$

Projecting (60) onto the kth structure mode ξ_k in the $L^2(\partial\Omega)$ inner product gives

$$\begin{pmatrix} \dot{b}_k \\ \ddot{b}_k \end{pmatrix} + \underbrace{\begin{pmatrix} 0 & -1 \\ \mathscr{D}(\xi_k, \nabla^4\xi_k)_{L^2(\partial\Omega)} & 0 \end{pmatrix}}_{\equiv \mathbf{G}_k} \begin{pmatrix} b_k \\ \dot{b}_k \end{pmatrix} = 0. \tag{61}$$

Let the energy associated with the Galerkin projection of the structure-only plate ROM $\dot{\mathbf{s}} = \mathbf{D}\mathbf{s}$ be defined by

$$E_p \equiv \frac{1}{2}||\mathbf{r}_P||^2_{L^2(\partial\Omega)} = \frac{1}{2}\int_{\partial\Omega} \mathbf{r}_P^{\mathrm{T}}\mathbf{r}_P \,\mathrm{d}S. \tag{62}$$

Then, the rate of change in energy of the structure-only system is

$$\begin{aligned}
\frac{1}{2}\frac{\mathrm{d}}{\mathrm{d}t}||\mathbf{r}_P||^2_{L^2(\partial\Omega)} &= \frac{1}{2}\frac{\mathrm{d}}{\mathrm{d}t}\int_{\partial\Omega} \mathbf{r}_P^{\mathrm{T}}\mathbf{r}_P \,\mathrm{d}S \\
&= \frac{1}{2}\frac{\mathrm{d}}{\mathrm{d}t}\int_{\partial\Omega} \left\{ \sum_{k=1}^{P}\sum_{l=1}^{P} (\xi_k, \xi_l)_{L^2(\partial\Omega)} \begin{pmatrix} b_k & \dot{b}_k \end{pmatrix} \begin{pmatrix} b_l \\ \dot{b}_l \end{pmatrix} \right\} \mathrm{d}S \\
&= \frac{1}{2}\frac{\mathrm{d}}{\mathrm{d}t}\int_{\partial\Omega} \left\{ \sum_{k=1}^{P}\sum_{l=1}^{P} \delta_{kl} \begin{pmatrix} b_k & \dot{b}_k \end{pmatrix} \begin{pmatrix} b_l \\ \dot{b}_l \end{pmatrix} \right\} \mathrm{d}S \\
&= \frac{1}{2}\frac{\mathrm{d}}{\mathrm{d}t}\int_{\partial\Omega} \left\{ \sum_{k=1}^{P} \begin{pmatrix} b_k & \dot{b}_k \end{pmatrix} \begin{pmatrix} b_k \\ \dot{b}_k \end{pmatrix} \right\} \mathrm{d}S \\
&= \int_{\partial\Omega} \sum_{k=1}^{P} \begin{pmatrix} b_k & \dot{b}_k \end{pmatrix} \begin{pmatrix} \dot{b}_k \\ \ddot{b}_k \end{pmatrix} \mathrm{d}S \\
&= \sum_{k=1}^{P} \begin{pmatrix} b_k & \dot{b}_k \end{pmatrix} \underbrace{\begin{pmatrix} 0 & 1 \\ -\omega_k^2 & 0 \end{pmatrix}}_{-\mathbf{G}_k} \begin{pmatrix} b_k \\ \dot{b}_k \end{pmatrix} \mathrm{d}S,
\end{aligned} \tag{63}$$

DOI: 10.1002/nme

where δ_{kl} denotes the usual Krönecker delta function, the definition $\omega_k^2 \equiv \mathscr{D}(\xi_k, \nabla^4 \xi_k)_{L^2(\partial\Omega)}$ has been employed. The Lyapunov condition for stability (Section A.4 in the Appendix) is that the real parts of the eigenvalues of the matrices $\{-\mathbf{G}_k : k = 1, 2, \ldots, P\}$ must be nonpositive. The eigenvalues of these matrices are $\pm\sqrt{-\omega_k^2} = \pm i\sqrt{\omega_k^2}$, where $i \equiv \sqrt{-1}$ because $\omega_k^2 \geqslant 0$ for all K. Because the eigenvalues are all pure imaginary or 0, the Lyapunov condition holds, which implies that the last line of (63) is $\leqslant 0$, as desired. It follows that the Galerkin projection of the plate equation (23) in the $L^2(\partial\Omega)$ inner product is stable. □

Recalling the definition of the energy of the fluid and structure ROMs (49) and (62), respectively, the total energy of the Galerkin projection of the coupled system is defined as

$$E_T \equiv \frac{1}{2}||\mathbf{q}'_M||^2_{(\mathbf{H},\Omega)} + \frac{1}{2}||\mathbf{r}_P||^2_{L^2(\partial\Omega)} = \begin{pmatrix} \mathbf{q}'^{\mathrm{T}}_M & \mathbf{r}^{\mathrm{T}}_P \end{pmatrix} \begin{pmatrix} \frac{1}{2}\mathbf{H} & \mathbf{0} \\ \mathbf{0} & \frac{1}{2}\mathbf{I}_2\delta_{\partial\Omega} \end{pmatrix} \begin{pmatrix} \mathbf{q}'_M \\ \mathbf{r}_P \end{pmatrix}, \tag{64}$$

where $\mathbf{I}_2$ denotes the 2×2 identity matrix and where $\delta_{\partial\Omega}$ is an indicator function marking the plate boundary $\partial\Omega$:

$$\delta_{\partial\Omega} \equiv \begin{cases} 1, & \text{for } \mathbf{x} \in \partial\Omega, \\ 0, & \text{otherwise.} \end{cases} \tag{65}$$

The following theorem shows that, under certain physical assumptions about the flow field and the pressure loading, $\frac{\mathrm{d}E_T}{\mathrm{d}t} \leqslant 0$, which implies stability for the Galerkin projection of the coupled fluid/structure system (45).

Theorem 4.3.3
Assume the base flow field satisfies a no-penetration condition on the plate ($\bar{u}_n = 0$), the base flow is uniform ($\nabla\bar{\mathbf{q}} = \mathbf{0}$), and the acoustically reflecting boundary condition (34) is applied on $\partial\Omega$. Assume in addition that $\bar{u} = 0$ at the plate. If the fluid pressure loading is

$$g = -p'_M + K\left(u'_{n,M} - u'_p\right) \quad \text{on} \quad \partial\Omega, \tag{66}$$

with $K = -\bar{\rho}\bar{c}$, then $\frac{\mathrm{d}E_T}{\mathrm{d}t} \leqslant 0$ (with $\frac{\mathrm{d}E_T}{\mathrm{d}t}$ defined in (68)). In other words, the Galerkin projection of the coupled fluid/structure system (45) is stable if the fluid equations (2) are projected in the $(\mathbf{H}, \Omega)$ inner product, and the plate equation (23) is projected in the $L^2(\partial\Omega)$ inner product.

Proof
First, observe

$$-\bar{\rho}\bar{c}u'^2_{n,M} = -\bar{\rho}\bar{c}\left(u'_{n,M} - u'_p\right)^2 - 2\bar{\rho}\bar{c}u'_p\left(u'_{n,M} - u'_p\right) - \bar{\rho}\bar{c}u'^2_p, \tag{67}$$

(an identity). Note also that, under the assumption that $\bar{u} = 0$ at the plate, $u'_p \equiv -\dot{w} = -\mathbf{r}_P^{\mathrm{T}}\mathbf{e}_2$, where $\mathbf{e}_2^{\mathrm{T}} \equiv \begin{pmatrix} 0 & 1 \end{pmatrix}$. Then, from (55) and (60), and assuming a pressure loading of the form $g = -p'_M + K(u'_{n,M} - u'_p)$ for some constant $K \in \mathbb{R}$:

$$\begin{aligned}
\frac{\mathrm{d}E_T}{\mathrm{d}t} &= \frac{1}{2}\frac{\mathrm{d}}{\mathrm{d}t}||\mathbf{q}'_M||^2_{(\mathbf{H},\Omega)} + \frac{1}{2}\frac{\mathrm{d}}{\mathrm{d}t}||\mathbf{r}_P||^2_{L^2(\partial\Omega)} \\
&= \int_{\partial\Omega}\left[-\bar{\rho}\bar{c}u'^2_{n,M} - \left(\bar{\rho}\bar{c}u'_{n,M} - p'_M\right)\mathbf{r}_P^{\mathrm{T}}\mathbf{e}_2\right]\mathrm{d}S + \int_{\partial\Omega}\mathbf{r}_P^{\mathrm{T}}(-\mathbf{G}\mathbf{r}_P - p'_M\mathbf{e}_2)\mathrm{d}S \\
&= \int_{\partial\Omega}\left[-\bar{\rho}\bar{c}(u'_{n,M} - u'_p)^2 - 2\bar{\rho}\bar{c}u'_p(u'_{n,M} - u'_p) - \bar{\rho}\bar{c}u'^2_p - \left(\bar{\rho}\bar{c}u'_{n,M} - p'_M\right)\mathbf{r}_P^{\mathrm{T}}\mathbf{e}_2\right]\mathrm{d}S \\
&\quad + \int_{\partial\Omega}\mathbf{r}_P^{\mathrm{T}}(-\mathbf{G}\mathbf{r}_P + [-p'_M + K(u'_{n,M} - u'_p)]\mathbf{e}_2)\mathrm{d}S
\end{aligned}$$

DOI: 10.1002/nme

$$
\begin{aligned}
&= \int_{\partial\Omega} \Big[-\bar{\rho}\bar{c}\left(u'_{n,M} - u'_p\right)^2 - 2\bar{\rho}\bar{c}u'_p\left(u'_{n,M} - u'_p\right) - \bar{\rho}\bar{c}u'^2_p - \bar{\rho}\bar{c}u'_{n,M}u'_p - \mathbf{r}_P^{\mathrm{T}}\mathbf{G}\mathbf{r}_P \\
&\qquad -K\left(u'_{n,M} - u'_p\right)u'_p \Big] \mathrm{d}S \\
&= \int_{\partial\Omega} \Big[-\mathbf{r}_P^{\mathrm{T}}\mathbf{G}\mathbf{r}_P - \bar{\rho}\bar{c}\left(u'_{n,M} - u'_p\right)^2 - 2\bar{\rho}\bar{c}u'_p\left(u'_{n,M} - u'_p\right) + \bar{\rho}\bar{c}u'_p\left(u'_{n,M} - u'_p\right) \\
&\qquad -K\left(u'_{n,M} - u'_p\right)u'_p \Big] \mathrm{d}S \\
&= \int_{\partial\Omega} \Big[-\mathbf{r}_P^{\mathrm{T}}\mathbf{G}\mathbf{r}_P - \bar{\rho}\bar{c}\left(u'_{n,M} - u'_p\right)^2 - \bar{\rho}\bar{c}u'_p\left(u'_{n,M} - u'_b\right) - K\left(u'_{n,M} - u'_p\right)u'_p \Big] \mathrm{d}S.
\end{aligned}
\tag{68}
$$

If $K = -\bar{\rho}\bar{c}$, the $u'_p\left(u'_{n,N} - u'_p\right)$ terms cancel. Then

$$
\begin{aligned}
\frac{\mathrm{d}E_T}{\mathrm{d}t} &= \int_{\partial\Omega} \left[-\mathbf{r}_P^{\mathrm{T}}\mathbf{G}\mathbf{r}_P - \bar{\rho}c\left(u'_{n,M} - u'_p\right)^2 \right] \mathrm{d}S \\
&= \frac{\mathrm{d}E_p}{\mathrm{d}t} - \int_{\partial\Omega} \bar{\rho}\bar{c}\left(u'_{n,M} - u'_p\right)^2 \mathrm{d}S \\
&\leqslant 0,
\end{aligned}
\tag{69}
$$

provided the Galerkin projection of the plate structure-only system is stable, which it is by Lemma 4.3.2. □

4.4. Physical versus numerical stability and other stability considerations

A discussion of the physical implication of the result of Theorem 4.3.3 is in order. It is well known that transient FSI problems have one particularity: they possess a wide range of self-excited vibrations and instabilities. For example, at Mach numbers for which the speed of the flow is above the critical flutter speed [24, 47], the structural system extracts energy from the flow system, and a small accidental disturbance in the structure can trigger an instability or oscillation. These physical instabilities can occur even in the linear regime, such as the one considered here. The objective of a numerical stability analysis is to determine conditions under which the numerical discretization does not add any *non*physical instabilities into the computation. For the scenario considered in the present work, the relevant physical instability is flutter. For supersonic flow, it is well known that once $\bar{u}$ exceeds a certain threshold (the flutter speed), the system becomes linearly unstable – that is, flutter occurs (Section 5). The fact that $\bar{u} = 0$ on $\partial\Omega$ is a sufficient condition for stability (Theorem 4.3.3) is a physically sensible one: in the case when $\bar{u} = 0$, the structure cannot extract energy from the mean flow, as occurs in flutter (an instability). The FSI system may be stable for nonzero $\bar{u}$ at the plate as well; it is just not guaranteed to remain stable. Suppose the function g is the unperturbed pressure loading (33), so that $g = -p'_M$ on $\partial\Omega$. Then, assuming $\bar{u} = 0$ on the plate as in Theorem 4.3.3, the estimate (68) is

$$
\begin{aligned}
\frac{\mathrm{d}E_T}{\mathrm{d}t} &= \frac{1}{2}\frac{\mathrm{d}}{\mathrm{d}t}||\mathbf{q}'_M||^2_{(\mathbf{H},\Omega)} + \frac{1}{2}\frac{\mathrm{d}}{\mathrm{d}t}||\mathbf{r}_P||^2_{L^2(\partial\Omega)} \\
&= \int_{\partial\Omega} \left[-\bar{\rho}\bar{c}u'^2_{n,M} - \left(\bar{\rho}\bar{c}u'_{n,M} - p'_M\right)\mathbf{r}_P^{\mathrm{T}}\mathbf{e}_2 \right] \mathrm{d}S + \int_{\partial\Omega} \mathbf{r}_P^{\mathrm{T}}(-\mathbf{G}\mathbf{r}_P - p'_M\mathbf{e}_2)\mathrm{d}S \\
&= \int_{\partial\Omega} \left[\mathbf{e}_2^{\mathrm{T}}\left(-\bar{\rho}\bar{c}u'^2_{n,M}\right)\mathbf{e}_2 - \mathbf{r}_P^{\mathrm{T}}\mathbf{G}\mathbf{r}_P - \mathbf{r}_P^{\mathrm{T}}\bar{\rho}\bar{c}u'_{n,M}\mathbf{e}_2 \right] \mathrm{d}S \\
&= \frac{\mathrm{d}E_f}{\mathrm{d}t} + \frac{\mathrm{d}E_p}{\mathrm{d}t} + \int_{\partial\Omega} \bar{\rho}\bar{c}u'_{n,M}u'_p \mathrm{d}S.
\end{aligned}
\tag{70}
$$

Equation (68) implies that if there is a 'stability margin' in the fluid-only and/or structure-only systems (that is, if $\frac{\mathrm{d}E_f}{\mathrm{d}t} \leqslant 0$ and/or $\frac{\mathrm{d}E_p}{\mathrm{d}t} \leqslant 0$), the coupled system can still be stable as long as

$$
\int_{\partial\Omega} \bar{\rho}\bar{c}u'_{n,M}u'_p \mathrm{d}S \leqslant -\frac{\mathrm{d}E_f}{\mathrm{d}t} - \frac{\mathrm{d}E_p}{\mathrm{d}t}. \tag{71}
$$

DOI: 10.1002/nme

For $\bar{u} \neq 0$, an aeroelastic analysis proceeds by determining the conditions under which the eigenvalues of the system matrix (45) will have positive real part, that is, checking numerically the Lyapunov stability condition (Section A.4 of the Appendix), as carried out in Section 5.

Another physical scenario that warrants some discussion is the case when the base flow is nonuniform ($\nabla\bar{\mathbf{q}}$). In the proof of Lemma 4.3.1, it was assumed that the base flow is uniform. This condition is a sufficient condition for the stability of the fluid ROM and yields a clean energy stability analysis. In this case, the ROM is guaranteed to be energy stable. It is also guaranteed to be time stable, that is, the solutions will remain bounded as $t \to \infty$. The uniform base flow assumption is *not* a necessary condition for energy stability of the fluid ROM. In the case when the base flow is nonuniform ($\mathbf{C} \neq \mathbf{0}$ in the fluid system (2)), the result of Lemma 4.3.1 still holds, but the energy estimate (48) replaced with the energy estimate

$$E_f(T) \leqslant e^{\frac{1}{2}\beta T} E_f(0), \tag{72}$$

where

$$E_f(t) \equiv \frac{1}{2}||\mathbf{q}'_{\boldsymbol{M}}(\cdot,t)||_{(\mathbf{H},\Omega)}, \tag{73}$$

denotes the fluid system energy at time t, and β is an upper bound on the eigenvalues of the matrix

$$\mathbf{Q} \equiv \mathbf{H}^{-\mathrm{T}/2}\frac{\partial(\mathbf{H}\mathbf{A}_i)}{\partial x_i}\mathbf{H}^{-1/2} - \mathbf{H}^{1/2}\mathbf{C}\mathbf{H}^{-1/2} - (\mathbf{H}^{1/2}\mathbf{C}\mathbf{H}^{-1/2})^{\mathrm{T}}. \tag{74}$$

A derivation of this energy estimate can be found in Section A.5 of the Appendix. The energy estimate (72) establishes the semi-boundedness of the equations (2) in the $(\mathbf{H},\Omega)$ norm, from which it follows that the symmetry inner product $(\cdot,\cdot)_{(\mathbf{H},\Omega)}$ is an energy inner product for the linearized compressible Euler equations. The practical implication of this result is that the numerical solution of a fluid ROM constructed in the symmetry inner product will be bounded in a way that is consistent with the behavior of the exact solutions of the governing equations (2). In the case of a nonuniform base flow, the fluid system (2) may support instabilities. In this case, the symmetry ROM will be energy stable even if there are physical unbounded solutions as $t \to \infty$; it will be time stable provided the system has been linearized around a stable (not necessarily uniform) base state $\bar{\mathbf{q}}$.

4.5. Stability-preserving discrete implementation

The stability analysis of the preceding subsections has assumed that the integrals resulting from the projection of the governing equations onto the reduced basis modes are evaluated exactly in continuous form. At first glance, it appears there may be a problem translating this continuous result to the discrete setting. This apparent difficulty is reminiscent of a similar problem that appears in spectral methods, where spectral projections need to be computed exactly. The problem is resolved in a similar way as in the spectral method context, namely through the use of high-precision numerical quadrature. First, the snapshots and the POD basis modes are cast as a collection of, at the present time, piecewise-linear (C^0) finite elements. It is then possible to construct a numerical quadrature operator that computes exactly all continuous inner products arising from the continuous Galerkin projection of the equations onto the POD modes. For details of this quadrature operator for the fluid ROM and the structure ROM, the reader is referred to [18] and [43], respectively. The introduction of C^0 finite elements requires a relaxation of the smoothness requirements on $\mathbf{q}'$, $\mathbf{H}$, $\{\mathbf{A}_i\}_{i=1}^3$, and w. The projection integrals are then to be interpreted in the sense of distributions. Higher order finite element representations of the POD modes and snapshots are possible. If these are to be employed, the order of the quadrature rule must be increased to ensure that no error is introduced into the numerical computation of the relevant inner products.

DOI: 10.1002/nme

5. NUMERICAL EXAMPLE: SUPERSONIC FLUTTER PANEL

The performance of the proposed FSI ROM is now studied on a problem of inviscid, supersonic flow past a thin, square, elastic rectangular $L_x \times L_y$ plate that is aligned with the flow (Figure 1). The out-of-plane x_3-direction displacement $w(x_1, x_2, t)$ of the plate is governed by the linearized von Kármán equation (23). The fore and aft edges of the plate are clamped to the surrounding flat surface, and the side edges are simply supported (Figure 1). For a given flow Mach number, the panel will undergo flutter once the non-dimensional dynamic pressure parameter λ^* exceeds a threshold [24]. This parameter is defined as

$$\lambda^* = \frac{3\rho_f \Upsilon^2 L_x^3}{2\mathscr{D}\sqrt{M^2-1}}, \tag{75}$$

where M is the given Mach number and Υ is mean streamwise flow speed. For the quasi-steady aerodynamic theory, the fluid speed and fluid density are calculated from $\Upsilon = \bar{c}M$ and $\rho_f = \frac{\rho_s h M}{10}$, where $\bar{c}$ is the mean speed of sound in the fluid. The values of the system parameters employed in generating the results presented herein are summarized in Table I. A numerical test case in which the base flow is uniform is selected simply because it allows for a verification of the method against a theoretical solution. Per the discussion in Section 4.4, the uniform base flow assumption is not required for the stability of the fluid, and therefore the coupled, ROM. Numerical experiments verifying the stability properties of a fluid ROM constructed in the symmetry inner product under a nonuniform base flow have been the subject of some recent work by Serre *et al.*, and the reader interested in numerical results involving the nonuniform base flow case is referred to [20].

For this problem, a fluid POD basis was obtained from a set of snapshots of a high-fidelity solution computed using the AERO-F simulation code, run in 'Linearized Euler' mode with a uniform base flow, and a free stream Mach number of 2.0. The computational fluid mesh is shown in Figure 2. The reader may observe by examining this figure that the grid nodes are clustered around the square panel location on the bottom surface of the mesh. The fluid POD reduced basis was computed from the complex-valued AERO-F fluid solutions using the frequency domain POD algorithm described in [25, 26].

Table I. System parameters for the fluid–structure interaction problem in Section 5.

Variable	Value
Plate modulus of elasticity, E	75.378 GPa
Plate thickness, h	4.66 mm
Plate length in the downstream direction, L_x	1 M
Plate length in the cross-stream direction, L_y	1 M
Plate density, ρ_s	2770 kg/m^3
Poisson's ratio of the plate, ν	0.33
Mach number, M	2
Number of plate modes, P	15

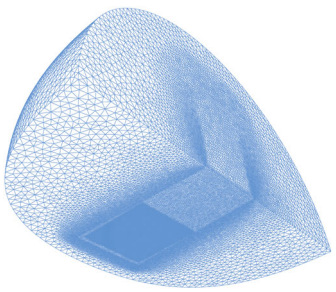

Figure 2. Computational mesh for the supersonic panel flutter problem.

DOI: 10.1002/nme

The motion of the linear von Kármán plate was described by four linear eigenmodes, computed using the ABAQUS software package [49] for a nonlinear place. A series of solutions for the fluid motion were obtained in the frequency domain, assuming time harmonic oscillation of each of the plate modes over a range of discrete frequencies. The non-dimensional frequencies for the computations were equally spaced from 0 to 8.0 at intervals of 0.04. The linear perturbations of the plate eigenmodes provided forcing for the solution in the fluid domain. A particular solution for an oscillatory plate motion is shown in Figure 3.

The coupled ROM was constructed by projecting the linearized Euler equations onto the aforementioned POD basis and incorporating the boundary coupling terms using the methods described in Section 4.2. The stabilization term derived in Theorem 4.3.3 to guarantee stability was not added to the pressure loading for this example. The FSI system (45) was advanced forward in time using an implicit fourth-order Runge–Kutta integration scheme. An *a posteriori* stability analysis was performed by computing the eigenvalues of the resulting ROM system matrix and examining the maximum real component of the eigenvalues, that is, by checking numerically the Lyapunov stability condition (Section A.4 of the Appendix). For all coupled ROMs, $P = 15$ plate modes were employed. Figure 4 compares the results of this analysis for 32, 48, and 64 fluid mode ROMs and for the theoretical result using quasi-steady aerodynamic theory, also called piston theory. 'Piston theory' refers to early studies of fluid-plate coupling in which one assumes a quasi-steady fluid flow model that allows for the effect of the fluid on the plate to be modeled as being dependent on the plate's velocity of vibration and slope in the flow's direction [24]. With sufficient resolution, the

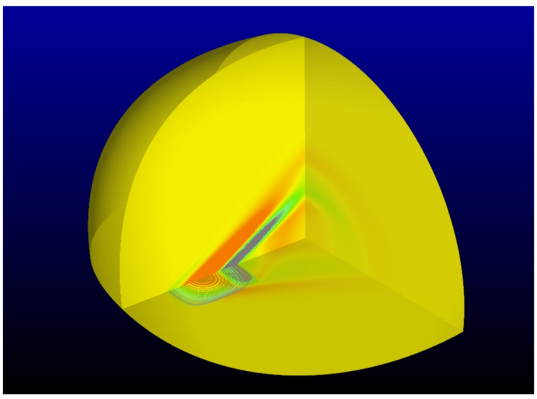

Figure 3. Pressure fluctuation field for harmonic oscillation of the first panel eigenmode (continuous contours) and plate deflection (line contours).

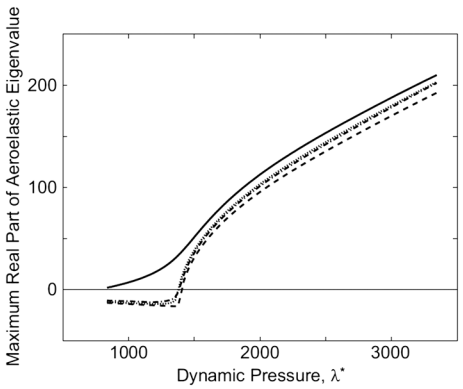

Figure 4. Panel flutter analysis using the coupled ROM compared with predictions using aerodynamic piston theory for the plate with properties listed in Table I; displayed are the (–) 32 mode fluid ROM, (– · –) 48 mode fluid ROM, (· · ·) 64 mode fluid ROM, and (––) piston theory.

DOI: 10.1002/nme

ROM properly predicts the maintenance of stability below the boundary and a reasonable prediction for the instability growth rate above the flutter boundary. The reader may observe that the ROM solution converged by 48 fluid modes, giving a result for the flutter dynamic pressure within 5% of the theoretical value. The reader may also observe that the 48 mode fluid ROM agrees better with the piston theory result plotted in Figure 4 than the 64 mode ROM for unstable conditions. As aerodynamic piston theory is valid for $M >> 1$, small differences between this theory and the solutions to the linearized Euler equations are expected at the Mach number considered. Numerical error in the full-order CFD solution, inherited by the ROM, may also lead to discrepancies with the theory. Further comparisons reveal that, whereas the 48 mode ROM agrees better with theory for unstable conditions than the 64 mode ROM, the 64 mode ROM agrees better with the theory for stable solutions.

The results for this numerical example are consistent with the discussion in Section 4.4. For small $\bar{u}$, λ^* is small, so linear stability of the system is to be expected, as the system does not extract enough energy from the mean flow to go unstable. Above a certain threshold $\bar{u}$ (or λ^*), however, the plate undergoes flutter and an instability forms. Figure 4 also suggests that the stability margin in the ROM without the perturbed pressure loading required for stability (Theorem 4.3.3), that is, the right-hand size of (71), is large enough for this problem for the ROM to remain numerically stable in a way that is consistent with piston theory below the threshold λ^* at which flutter occurs. These observations are further evidence that the result of Theorem 4.3.3 is a sufficient but not a necessary condition for linear stability of the coupled fluid and structure ROM.

6. CONCLUSIONS

A ROM for an FSI problem involving linearized compressible fluid flow coupled with a linearized von Kármán plate equation is developed. The fluid model is constructed by first calculating a reduced basis via the POD, then taking the Galerkin projection of the governing equations onto this basis using a stability-preserving 'symmetry' inner product constructed specifically for these equations [18, 19]. The structural modes are taken to be the eigenmodes of the governing linearized plate equation. The structure ROM is also constructed via a Galerkin projection, but in the standard L^2 inner product. Both ROMs are built using the continuous Galerkin projection approach: the Galerkin projection step is applied to the original continuous equations rather than their discretized analogs. This approach enables an *a priori* stability analysis of each of the ROMs, as well as the coupled fluid and structure ROM resulting from applying appropriate boundary conditions at the plate boundary. Stability of the Galerkin projection of the fluid-only and structure-only equations is proven. These results are then employed to derive sufficient conditions for linear stability of the coupled fluid/structure system under certain physical assumptions. The conditions derived connect naturally to the physics of the problem, for example, the existence of a 'flutter boundary' at which the physical system goes unstable, and flutter is known to occur. It is shown that stability can be maintained by adding a stabilization-like term to the fluid pressure loading imposed on the plate equations. The coupled model is verified against results from classical piston theory on a numerical example for which the plate will undergo flutter above a certain threshold dynamic pressure parameter. Stability of the FSI ROM is checked numerically *a posteriori*. The ROM remains stable for values below the flutter boundary and is shown to have a reasonable prediction for the instability growth rate above the flutter boundary.

APPENDIX A

A.1. Diagonalization of $\mathbf{A}_n$

Let $\mathbf{A}_n \equiv \mathbf{A}_1 n_1 + \mathbf{A}_2 n_2 + \mathbf{A}_3 n_3$. The reader may verify that the matrices $\mathbf{S}$ that diagonalize $\mathbf{A}_n$ (so that $\mathbf{A}_n = \mathbf{S}\boldsymbol{\Lambda}_n\mathbf{S}^{-1}$, with $\boldsymbol{\Lambda}_n$ given in (5)) are as follows:

DOI: 10.1002/nme

$$\mathbf{S}=\begin{pmatrix} 0 & n_3 & n_2 & \frac{1}{2}n_1 & -\frac{1}{2}n_1 \\ n_3 & 0 & -n_1 & \frac{1}{2}n_2 & -\frac{1}{2}n_2 \\ -n_2 & -n_1 & 0 & \frac{1}{2}n_3 & -\frac{1}{2}n_3 \\ n_1 & -n_2 & n_3 & -\frac{\bar{\xi}}{2\bar{c}} & -\frac{\bar{\xi}}{2\bar{c}} \\ 0 & 0 & 0 & \frac{\gamma\bar{p}}{2\bar{c}} & \frac{\gamma\bar{p}}{2\bar{c}} \end{pmatrix}, \quad \mathbf{S}^{-1}=\begin{pmatrix} 0 & n_3 & -n_2 & n_1 & \frac{\bar{\xi}}{\gamma\bar{p}}n_1 \\ n_3 & 0 & -n_1 & -n_2 & -\frac{\bar{\xi}}{\gamma\bar{p}}n_2 \\ n_2 & -n_1 & 0 & n_3 & \frac{\bar{\xi}}{\gamma\bar{p}}n_3 \\ n_1 & n_2 & n_3 & 0 & \frac{\bar{c}}{\gamma\bar{p}} \\ -n_1 & -n_2 & -n_3 & 0 & \frac{\bar{c}}{\gamma\bar{p}} \end{pmatrix}. \tag{A.1}$$

A.2. System matrices for coupled fluid–structure interaction reduced order model

In Section 4.3, it was shown that the linearized coupled fluid and structure ROM system has the form

$$\begin{pmatrix} \dot{\mathbf{f}} \\ \dot{\mathbf{s}} \end{pmatrix}=\begin{pmatrix} \mathbf{A} & \mathbf{B} \\ \mathbf{C} & \mathbf{D} \end{pmatrix}\begin{pmatrix} \mathbf{f} \\ \mathbf{s} \end{pmatrix}. \tag{A.2}$$

Here, the entries of the matrices that appear in (A.2) are given. Begin by writing (A.2) as

$$\begin{pmatrix} \dot{\mathbf{a}} \\ \dot{\mathbf{b}} \\ \ddot{\mathbf{b}} \end{pmatrix}=\left(\begin{array}{c|cc} \mathbf{A} & \hat{\mathbf{B}}^1 & \hat{\mathbf{B}}^2 \\ \hline \mathbf{0} & \mathbf{0} & \mathbf{I} \\ \hat{\mathbf{C}} & \hat{\mathbf{D}} & \mathbf{0} \end{array}\right)\begin{pmatrix} \mathbf{a} \\ \mathbf{b} \\ \dot{\mathbf{b}} \end{pmatrix}, \tag{A.3}$$

where $\mathbf{a}\equiv\mathbf{f}$ and $\mathbf{b}^{\mathrm{T}}\equiv\begin{pmatrix} b_1(t), & \cdots, & b_P(t) \end{pmatrix}\in\mathbb{R}^P$.

Then, from (42) and (44), the entries of the matrices that appear in (A.2) are as follows:

$$A_{jk}=-\left(\boldsymbol{\phi}_j,\mathbf{A}_i\frac{\partial\boldsymbol{\phi}_k}{\partial x_i}+\mathbf{C}\boldsymbol{\phi}_k\right)_{(\mathbf{H},\Omega)}-\int_{\partial\Omega}\bar{\rho}\bar{c}\boldsymbol{\phi}_j^n\phi_k^n\mathrm{d}S, \qquad j,k=1,\ldots,M, \tag{A.4}$$

$$\hat{B}^1_{jk}=-\int_{\partial\Omega}\bar{\rho}\bar{c}\bar{u}\phi_j^n\frac{\partial\xi_k}{\partial x_1}\,\mathrm{d}S, \quad j=1,\ldots,M,k=1,\ldots,P, \tag{A.5}$$

$$\hat{B}^2_{jk}=-\int_{\partial\Omega}\bar{\rho}\bar{c}\phi_j^n\xi_k\,\mathrm{d}S, \quad j=1,\ldots,M,k=1,\ldots,P, \tag{A.6}$$

$$\hat{C}_{jk}=-\int_{\partial\Omega}\phi_k^5\xi_j\mathrm{d}S, \quad j=1,\ldots,P,k=1,\ldots,M, \tag{A.7}$$

$$\hat{D}_{jk}=\begin{cases} -\mathscr{D}\int_{\partial\Omega}\nabla^4\xi_j\xi_k\mathrm{d}S, & j,k=1,\ldots,P,j=k, \\ 0, & \text{otherwise}, \end{cases} \tag{A.8}$$

and where $\mathbf{0}$ and $\mathbf{I}$ denote the zero and identity matrices, respectively.

A.3. Stability

Consider a general IBVP of the form

$$\begin{aligned} \frac{\partial u}{\partial t}&=Pu+F, \ \ t\geqslant 0, \\ Bu&=g, \\ u&=f, \qquad\quad t=0. \end{aligned} \tag{A.9}$$

Here, P is a differential operator in space, and B is a boundary operator acting on the solution at the spatial boundary.

DOI: 10.1002/nme

Definition 2.11 in [48]: The semi-discrete IBVP resulting from the semi-discretization of (A.9) is *stable* if there is a unique solution satisfying

$$||u(\cdot,t)||_h \leqslant Ke^{\alpha t}||f(\cdot)||_h, \tag{A.10}$$

where K and α are constants independent of f and g.

It is common to use energy estimates to check for stability, if

$$\frac{\mathrm{d}}{\mathrm{d}t}||u(\cdot,t)||_h^2 \leqslant 0, \tag{A.11}$$

then (A.10) is satisfied, and we have stability.

A.4. Lyapunov stability condition

A continuous-time linear time-invariant system $\dot{\mathbf{x}} = \mathbf{A}\mathbf{x}$ is Lyapunov stable if and only if all the eigenvalues of $\mathbf{A}$ have real parts less than or equal to 0, and those with real parts equal to 0 are non-repeated (see, for instance, [30]).

A.5. Energy stability of the fluid reduced order model in the symmetry inner product: nonuniform base flow case

Theorem 6.1

Assume the base flow field satisfies a no-penetration condition on the plate ($\bar{u}_n = 0$) and there is a general (nonuniform) base flow $\bar{\mathbf{q}}$. Then the Galerkin projection of the linearized compressible Euler equations (2) in the symmetry inner product $(\mathbf{H}, \Omega)$ with the linearized acoustically reflecting boundary condition (34) is stable for the fluid ROM, with energy estimate

$$||\mathbf{q}'_M(\cdot,T)_{(\mathbf{H},\Omega)} \leqslant e^{\frac{1}{2}\beta T}||\mathbf{q}'_M(\cdot,0)||_{(\mathbf{H},\Omega)}, \tag{A.12}$$

where β is an upper bound on the eigenvalues of the matrix

$$\mathbf{Q} \equiv \mathbf{H}^{-\mathrm{T}/2}\frac{\partial(\mathbf{H}\mathbf{A}_i)}{\partial x_i}\mathbf{H}^{-1/2} - \mathbf{H}^{1/2}\mathbf{C}\mathbf{H}^{-1/2} - (\mathbf{H}^{1/2}\mathbf{C}\mathbf{H}^{-1/2})^{\mathrm{T}}. \tag{A.13}$$

and $\mathbf{q}'_M$ is given by (17). It follows that the discrete fluid-only ROM system $\dot{\mathbf{f}} = \mathbf{A}\mathbf{f}$ is stable provided the continuous system (2) is a stable regime.

Proof

$$\begin{aligned}
\frac{1}{2}\frac{\mathrm{d}}{\mathrm{d}t}||\mathbf{q}'_M||^2_{(\mathbf{H},\Omega)} &= \frac{1}{2}\frac{\mathrm{d}}{\mathrm{d}t}(\mathbf{q}'_M, \mathbf{q}'_M)_{(\mathbf{H},\Omega)} \\
&= \int_\Omega \mathbf{q}'^{\mathrm{T}}_M \mathbf{H}\frac{\partial \mathbf{q}'_M}{\partial t}d\Omega \\
&= -\int_\Omega \mathbf{q}'^{\mathrm{T}}_M \mathbf{H}\left[\mathbf{A}_i\frac{\partial \mathbf{q}'_M}{\partial x_i} + \mathbf{C}\mathbf{q}'\right]\mathrm{d}\Omega \\
&= -\int_{\partial\Omega} \mathbf{q}'^{\mathrm{T}}_M \mathbf{H}\mathbf{A}_n\mathbf{q}'_p\,\mathrm{d}S + \frac{1}{2}\int_\Omega \frac{\partial}{\partial x_i}\left(\mathbf{q}'^{\mathrm{T}}_M \mathbf{H}\mathbf{A}_i\mathbf{q}'_M\right)\mathrm{d}\Omega \\
&\quad + \frac{1}{2}\int_\Omega \mathbf{q}'^{\mathrm{T}}_M\left[\frac{\partial(\mathbf{H}\mathbf{A}_i)}{\partial x_i} - 2\mathbf{H}\mathbf{C}\right]\mathbf{q}'_M\,\mathrm{d}\Omega \\
&= -\int_{\partial\Omega} \mathbf{q}'^{\mathrm{T}}_M \mathbf{H}\mathbf{A}_n\mathbf{q}'_p\,\mathrm{d}S + \frac{1}{2}\int_{\partial\Omega} \mathbf{q}'^{\mathrm{T}}_M \mathbf{H}\mathbf{A}_n\mathbf{q}'_M\,\mathrm{d}S \\
&\quad + \frac{1}{2}\int_\Omega \mathbf{q}'^{\mathrm{T}}_M\left[\frac{\partial(\mathbf{H}\mathbf{A}_i)}{\partial x_i} - \mathbf{H}\mathbf{C} - \mathbf{C}^T\mathbf{H}\right]\mathbf{q}'_M\,\mathrm{d}\Omega \\
&= \int_{\partial\Omega} \mathbf{q}'^{\mathrm{T}}_M \mathbf{H}\mathbf{A}_n\left(\frac{1}{2}\mathbf{q}'_M - \mathbf{q}'_p\right)\mathrm{d}S + \frac{1}{2}\int_\Omega \mathbf{q}'^{\mathrm{T}}_M \mathbf{H}^{\mathrm{T}/2}\mathbf{Q}\mathbf{H}^{1/2}\mathbf{q}'^{\mathrm{T}}_M\mathrm{d}\Omega,
\end{aligned} \tag{A.14}$$

DOI: 10.1002/nme

where the matrix $\mathbf{Q}$ is defined in (A.13). In going from line three to line four in (A.14), the property that the $\mathbf{HA}_i$ for $i = 1, 2, 3$ are all symmetric has been invoked, as in the proof of Lemma 4.3.1.

Substituting the boundary conditions exactly as in the proof of Lemma 4.3.1 gives

$$\frac{1}{2}\frac{\mathrm{d}}{\mathrm{d}t}||\mathbf{q}'_M||^2_{(\mathbf{H},\Omega)} \leqslant \frac{1}{2}\int_\Omega \mathbf{q}'^{\mathrm{T}}_M \mathbf{H}^{\mathrm{T}/2}\mathbf{Q}\mathbf{H}^{1/2}\mathbf{q}'^{\mathrm{T}}_M \mathrm{d}\Omega, \tag{A.15}$$

or

$$\frac{\mathrm{d}}{\mathrm{d}t}||\mathbf{q}'_M||^2_{(\mathbf{H},\Omega)} \leqslant \beta||\mathbf{q}'_M||^2_{(\mathbf{H},\Omega)}. \tag{A.16}$$

Applying Gronwall's lemma to (A.16) gives the energy estimate (A.12). □

ACKNOWLEDGEMENTS

This research was funded by Sandia National Laboratories Laboratory Directed Research and Development (LDRD) program. Sandia is a multiprogram laboratory operated by Sandia Corporation, a Lockheed Martin Company for the United States Department of Energy's National Nuclear Security Administration under contract DE-AC04-94AL85000. The authors also gratefully acknowledge Thuan Lieu and Charbel Farhat of Stanford University for providing us with the AERO-F code and associated user-support.

REFERENCES

1. Holmes P, Lumley JL, Berkooz G. *Turbulence, Coherent Structures, Dynamical Systems and Symmetry*. Cambridge University Press: New York, NY, 1996.
2. Sirovich L. Turbulence and the dynamics of coherent structures, part III: dynamics and scaling. *Quarterly of Applied Mathematics* 1987; **45**(3):583–590.
3. Aubry N, Holmes P, Lumley J, Stone E. The dynamics of coherent structures in the wall region of a turbulent boundary layer. *Journal of Fluid Mechanics* 1988; **192**:115–173.
4. Veroy K, Patera AT. Certified real-time solution of the parametrized steady incompressible Navier–Stokes equations: rigorous reduced-bases a posteriori error bounds. *International Journal for Numerical Methods in Fluids* 2005; **47**:773–788.
5. Moore B. Principal component analysis in linear systems: controllability, observability, and model reduction. *IEEE Transactions on Automatic Control* 1981; **26**(1):17–32.
6. Gugercin S, Antoulas AC. A survey of model reduction by balanced truncation and some new results. *International Journal of Control* 2004; **77**(8):748–766.
7. Willcox K, Peraire J. Balanced model reduction via the proper orthogonal decomposition. *AIAA Journal* 2002; **40**(11):2323–2330.
8. Rowley CW. Model reduction for fluids using balanced proper orthogonal decomposition. *International Journal of Bifurcation and Chaos* 2005; **15**(3):997–1013.
9. Bui-Thanh T, Willcox K, Ghattas O, van Bloemen Waanders B. Goal-oriented, model constrained optimization for reduction of large-scale systems. *Journal of Computational Physics* 2007; **224**:880–896.
10. Milman MH, Chu C-C. Optimization methods for passive damper placement and tuning. *Journal of Guidance, Control & Dynamics* 1994; **17**:262–281.
11. Castanier MP, Tan Y-C, Pierre C. Characteristic constraint modes for component mode synthesis. *AIAA Journal* 2001; **39**:1182–1187.
12. Tan Y-C, Pierre C. Characteristic constraint modes for component mode synthesis. *AIAA Journal* 2005; **43**: 1360–1370.
13. Segalman DJ. Model reduction of systems with localized nonlinearities. *ASME Journal of Computational & Nonlinear Dynamics* 2007; **2**:249–266.
14. Hung ES, Senturia SD. Generating efficient dynamical models for microelectomechanical systems from a few finite-element simulation runs. *IEEE Journal of Microelectromechanical Systems* 1999; **8**:280–289.
15. Ribeiro P, Petyt M. Nonlinaer vibration of plates by the hierarchical finite element and continuiation methods. *International Journal of Mechanical Sciences* 1999; **41**:437–459.
16. Zhao X, Abdel-Rahman EM, Nayfeh AH. A reduced-order model for electrically actuated microplates. *Journal of Micromechanics & Microengineering* 2004; **14**:900–906.
17. Rowley CW, Colonius T, Murray RM. Model reduction for compressible flows using POD and Galerkin projection. *Physica D* 2004; **189**:115–129.
18. Barone MF, Kalashnikova I, Segalman DJ, Thornquist HK. Stable Galerkin reduced order models for linearized compressible flow. *Journal of Computational Physics* 2009; **228**:1932–1946.
19. Kalashnikova I, Barone MF. On the stability and convergence of a Galerkin reduced order model (ROM) for compressible flow with solid wall and far-field boundary treatment. *International Journal for Numerical Methods in Engineering* 2010; **87**:309–335.

DOI: 10.1002/nme

20. Serre G, Lafon P, Gloerfelt X, Bailly C. Reliable reduced-order models for time-dependent linearized Euler equations. *Journal of Computational Physics* 2012; **231**(15):5176–5194.
21. Kalashnikova I, Barone MF. Efficient non-linear proper orthogonal decomposition/Galerkin reduced order models with stable penalty enforcement of boundary conditions. *Int. J. Num. Meth. Engng.* 2012; **90**(11):1337–1362.
22. Amsallem D, Farhat C. Stabilization of projection-based reduced-order models. *International Journal for Numerical Methods in Engineering* 2012; **91**:358–377.
23. Bond BN, Daniel L. Guaranteed stable projection-based model reduction for indefinite and unstable linear systems. *Proceedings of the 2008 IEEE/ACM International Conference on Computer-Aided Design*, San Jose, CA, 2008; 728–735.
24. Dowell EH, Hall KC. Modeling of fluid structure interaction. *Annual Review of Fluid Mechanics and Engineering* 2001; **33**:445–490.
25. Lieu T, Farhat C, Lesoinne M. Reduced-order fluid/structure modeling of a complete aircraft configuration. *Computer Methods in Applied Mechanicas and Engineering* 2006; **195**:5730–5742.
26. Lieu T, Farhat C, Lesoinne M. POD-based aeroelastic analysis of a complete F-16 configuration: ROM adaptation and demonstration. *AIAA Paper 2005–2295*, 2005.
27. Vierendeels J, Lanoye L, Degroote J, Verdonck P. Implicit coupling of partitioned fluid-structure interaction problems with reduced order models. *Computers & Structures* 2007; **85**(11-14):970–976.
28. Hirt CW, Amsdem AA, Cook JL. An arbitrary Lagrangian–Eulerian computing method for all flow speeds. *Journal of Computational Physics* 1974; **14**:227–253.
29. Gustafsson B, Kreiss HO, Oliger J. *Time Dependent Problems and Difference Methods*. John Wiley & Sons, Inc.: New York, NY, 1995.
30. Chen G. *Stability of Nonlinear Systems. Encyclopedia of RF and Microwave Engineering*. Wiley: NY, 2004.
31. Gustafsson B, Sundstrom A. Incompletely parabolic problems in fluid dynamics. *SIAM Journal on Applied Mathematics* 1978; **35**(2):343–357.
32. Oliger J, Sundstrom A. Theoretical and practical aspects of some initial boundary value problems in fluid dynamics. *SIAM Journal on Applied Mathematics* 1978; **35**(3):419–446.
33. Lumley JL. *Stochastic Tools in Turbulence*. Academic Press: New York, NY, 1971.
34. Rathinam M, Petzold LR. A new look at proper orthogonal decomposition. *SIAM Journal on Numerical Analysis* 2003; **41**(5):1893–1925.
35. Kunisch K, Volkwein S. Galerkin proper orthogonal decomposition for a general equation in fluid dynamics. *SIAM J. Num. Anal.* 2002; **40**(2):492–515.
36. Barone MF, Kalashnikova I, Segalman DJ, Thornquist HK. Galerkin reduced order models for compressible flow with structural interaction. *AIAA 46th Aerospace Science Meeting and Exhibit, AIAA 2008-0612*, Reno, NV, 2008; 1–25.
37. Harten A. On the symmetric form of systems of conservation laws with entropy. *Journal of Computational Physics* 1983; **49**:151–164.
38. Hughes TJR, Franca LP, Mallet M. A new finite element formulation for computational fluid dynamics: I. symmetric forms of the compressible euler and Navier–Stokes equations and the second law of thermodynamics. *Computer Methods in Applied Mechanics and Engineering* 1986; **54**:223–234.
39. Bova SW, Carey GF. An entropy variable formulation and applications for the two-dimensional shallow water equations. *International Journal for Numerical Methods in Fluids* 1996; **23**:29–46.
40. Greven A, Keller G, Warnecke G. *Entropy*. Princeton University Press: Princeton, NJ, 2003.
41. Abarbanel S, Gottlieb D. Optimal time splitting for two- and three-dimensional Navier–Stokes equations with mixed derivatives. *Journal of Computational Physics* 1981; **35**:1–33.
42. Ziegler F. *Mechanics of Solids and Fluids*. Springer: New York, 1998.
43. Brake MR, Segalman DJ. Nonlinear model reduction of von Kármán plates under quasi-steady fluid flow. *AIAA Journal* 2010; **48**(10):2339–2347.
44. Brake MR, Barone MF, Segalman DJ. Nonlinear model reduction of von Kármán plates under linearized compressible flow. *AIAA Journal* 2011; **50**(5):1047–1059.
45. Leissa A. *Vibration of Plates*. The Acoustical Society of America: Washington, DC, 1993. (Originally issued by NASA, 1973).
46. Bisplinghoff RL, Ashley H. *Principles of Aeroelasticity*. Dover Publications Inc.: Mineola, NY, 2002.
47. Fung YC. *1G An Introduction to the Theory of Aeroelasticity*. Dover Publications: New York, NY, 1969, 160–185.
48. Gustafsson B. *High Order Difference Methods for Time Dependent PDE*. Springer-Verlag: Leipzig, Germany, 2008.
49. ABAQUS User's Manual (version 5.5). Hibbitt, Karlsson, and Sorensen, Inc., Pawtucker, U.S.A.

DOI: 10.1002/nme